Title

Unbiased Proteomic Profiling Uncovers a Targetable GNAS/PKA/PP2A Axis in Small Cell Lung Cancer Stem Cells

Journal

Cancer Cell, 38(1)

ISSN

1535-6108

Authors

Coles, Garry L

Cristea, Sandra

Webber, James T

et al.

Publication Date

2020-07-01

DOI

10.1016/j.ccell.2020.05.003

Peer reviewed

HHS Public Access

Author manuscript

Cancer Cell. Author manuscript; available in PMC 2021 July 13.

Published in final edited form as:

Cancer Cell. 2020 July 13; 38(1): 129–143.e7. doi:10.1016/j.ccell.2020.05.003.

UNBIASED PROTEOMIC PROFILING UNCOVERS A TARGETABLE GNAS/PKA/PP2A AXIS IN SMALL CELL LUNG CANCER STEM CELLS

Garry L. Coles[1,2], **Sandra Cristea**[1,2], **James T. Webber**[3], **Rebecca S. Levin**[4,5], **Steven M. Moss**[5], **Andy He**[1,2], **Jaya Sangodkar**[6], **Yeonjoo C. Hwang**[4,5,7], **Julia Arand**[1,2], **Alexandros P. Drainas**[1,2], **Nancie A. Mooney**[8,9], **Janos Demeter**[8,9], **Jessica N. Spradlin**[10], **Brandon Mauch**[1,2], **Vicky Le**[1,2], **Yan Ting Shue**[1,2], **Julie H. Ko**[1,2], **Myung Chang Lee**[1,2], **Christina Kong**[11], **Daniel K. Nomura**[10,12,13], **Michael Ohlmeyer**[14,15], **Danielle L. Swaney**[5,16,17], **Peter K. Jackson**[8,9], **Goutham Narla**[6], **John D. Gordan**[4,5,6], **Kevan Shokat**[4,5], **Julien Sage**[1,2,*]

[1]Department of Pediatrics, Stanford University, Stanford, CA 94305, USA

[2]Department of Genetics, Stanford University, Stanford, CA 94305, USA

[3]Department of Bioengineering and Therapeutic Sciences, University of California San Francisco, San Francisco, CA 94158, USA

[4]Howard Hughes Medical Institute, University of California San Francisco, San Francisco, CA 94158, USA

[5]Department of Cellular and Molecular Pharmacology, University of California San Francisco, San Francisco, CA 94158, USA

[6]Division of Genetic Medicine, Michigan Medicine, University of Michigan, Ann Arbor, MI, USA

[7]Department of Medicine, Helen Diller Family Comprehensive Cancer Center, University of California, San Francisco, San Francisco, CA 94143, USA

[*]Corresponding Author and Lead Contact: Julien Sage, Stanford University, 265 Campus Drive, Stanford, CA 94305-5457. Phone: 650-724-9246; Fax: 650-736-0195; julsage@stanford.edu.

AUTHOR CONTRIBUTIONS

Conceptualization, G.L.C., S.C., O.M., G.N., J.D.G., K.S., P.K.J., and Ju.S.; Formal Analysis, G.L.C., S.C., J.T.W., R.S.L., S.M.M., A.H., Ja.S., Y.C.H., J.A., A.P.D., M.C.L., D.L.S., G.N., J.D., J.D.G., K.S., and Ju.S.; Investigation, G.L.C., S.C., J.T.W., R.S.L., S.M.M., A.H., Ja.S., Y.H., B.M., V.L., Y.T.S., N.A.M., and J.D.G.; Resources: K.C., J.N.S., D.K.N., M.O.; Writing – Original Draft: G.L.C., S.C., and Ju.S.; Writing – Reviewing and Editing, all authors; Visualization, G.L.C., S.C., A.H., Ja.S., A.P.D., J.K., M.C.L, C.K., and Ju.S.; Supervision, D.K.N., G.N., P.K.J., J.D.G., K.S. and Ju.S.; Project Administration: Ju.S.; Funding Acquisition: D.K.N., M.O., G.N., P.K.J., J.D.G., K.S. and Ju.S.

DECLARATION OF INTEREST

M.O. acknowledges Partnership for New York City (PFNYC) for a BioAccelerate Award, funding large-scale synthesis of SMAP-1154. Mt Sinai has filed patents on behalf of M.O. on SMAP-1154 and SMAP-DT-061. CWRU has filed a patent on behalf of M.O. and G.N. describing combinations of '1154 and '061 with kinase inhibitors. The Icahn School of Medicine at Mount Sinai has filed patents covering composition of matter on the small molecules disclosed herein for the treatment of human cancer and other diseases (International Application Numbers: PCT/US15/19770, PCT/US15/19764; and US Patent: US 9,540,358 B2). RAPPTA Therapeutics LLC has optioned this intellectual property for the clinical and commercial development of this series of small molecule PP2A activators. G.N. has an ownership interest in RAPPTA Therapeutics LLC. DKN is a co-founder, share-holder, and scientific adviser for Artris Therapeutics and Frontier Medicines. J.S. receives research funding from Stemcentrx/Abbvie, Pfizer, and Revolution Medicines and owns stock in Forty Seven Inc.

[8]Baxter Laboratory, Stanford University, Stanford, CA 94305, USA

[9]Department of Microbiology & Immunology, Stanford University, Stanford, CA 94305, USA

[10]Department of Chemistry, University of California, Berkeley, Berkeley, CA 94720

[11]Department of Pathology, Stanford University, Stanford, CA 94305, USA

[12]Department of Molecular and Cell Biology, University of California, Berkeley, Berkeley, CA 94720

[13]Department of Nutritional Sciences and Toxicology, University of California, Berkeley, Berkeley, CA 94720

[14]Icahn School of Medicine at Mount Sinai, New York, New York, USA

[15]Atux Iskay LLC, Plainsboro, New Jersey, NJ 08536, USA

[16]Quantitative Biosciences Institute (QBI), University of California San Francisco, San Francisco, CA 94158, USA

[17]David J. Gladstone Institute, University of California San Francisco, San Francisco, CA 94158, USA

SUMMARY

Using unbiased kinase profiling, we identified protein kinase A (PKA) as an active kinase in small cell lung cancer (SCLC). Inhibition of PKA activity genetically, or pharmacologically by activation of the PP2A phosphatase, suppresses SCLC expansion in culture and *in vivo*. Conversely, GNAS (G-protein α subunit), a PKA activator that is genetically activated in a small subset of human SCLC, promotes SCLC development. Phosphoproteomic analyses identified many PKA substrates and mechanisms of action. In particular, PKA activity is required for the propagation of SCLC cancer stem cells in transplantation studies. Broad proteomic analysis of recalcitrant cancers has the potential to uncover targetable signaling networks, such as the GNAS/PKA/PP2A axis in SCLC.

Graphical Abstract

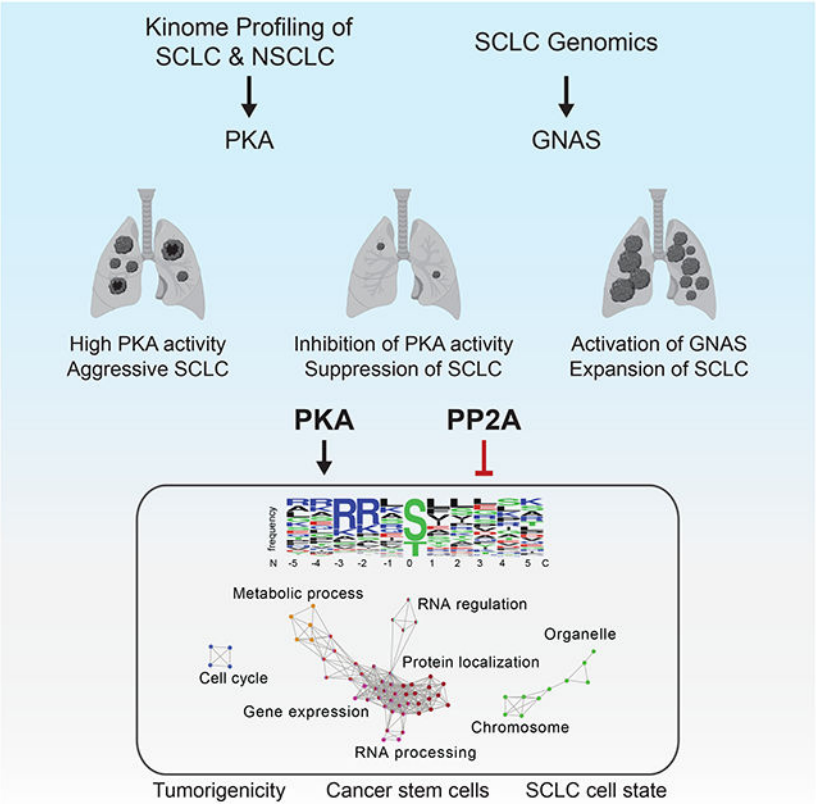

INTRODUCTION

Among all lung cancers, ~15% of cases show properties of neuroendocrine (NE) cells and are classified as small cell lung cancer (SCLC). SCLC development is usually associated with heavy smoking, and SCLC incidence is expected to increase in the next decades due to the increasing numbers of smokers. Worldwide, more than 200,000 people die from SCLC every year. SCLC tumors have a unique biology with a high proliferative and metastatic potential, resulting in very poor prognosis. The overall 5-year survival rate of SCLC patients is only 5-10%. Treatment options for SCLC patients have remained similar for the past 30 years with little improvement in these overall survival rates (reviewed in (Pietanza et al., 2015; Sabari et al., 2017)). Even immunotherapies successful in other cancer types have only limited efficacy in the vast majority of SCLC patients (Horn et al., 2018; Ready et al., 2019).

As with other cancers, a better understanding of the signaling pathways that drive the growth of SCLC tumors may eventually lead to the identification of improved therapeutic strategies. Unbiased genomic and transcriptomic studies often help identify such key drivers and key targets in cancer. In the case of SCLC, the sequencing of human tumors has begun to reveal some opportunities (George et al., 2015; Peifer et al., 2012; Rudin et al., 2012). First, SCLC tumors have nearly ubiquitous inactivation of genes coding for the RB and p53 tumor suppressors. This dual inactivation results in a dysregulated G1/S transition of the cell cycle, which has led to the idea that these tumors may display enhanced sensitivity to the

disruption of the G2/M transition. Indeed, inhibitors of G2/M kinases such as CHK1 and WEE1 may help inhibit the growth of SCLC (Doerr et al., 2017; Lallo et al., 2018; Sen et al., 2017a; Sen et al., 2017b). Second, RB loss and c-MYC up-regulation have been associated with increased sensitivity to specific therapies such as inhibitors of Aurora kinase (AURK) (Gay et al., 2019; Gong et al., 2019; Mollaoglu et al., 2017; Oser et al., 2019; Sos et al., 2012). Third, inactivating mutations in the acetyltransferase CREBBP may specifically increase sensitivity to inhibition of histone deacetylases (Jia et al., 2018).

Despite these encouraging examples, most recurrent genetic events in SCLC are not directly linked to obvious mechanisms of action, and these events do not readily identify therapeutic opportunities. It is possible that proteins encoded by genes not recurrently mutated could still play important roles in the proliferation and/or survival of SCLC cells. In particular, kinases and phosphatases are key signaling enzymes and are often effective therapeutic targets (Cohen, 2002; Vintonyak et al., 2009; Zhang et al., 2009). However, few recurrent genetic events seem to directly activate kinases in SCLC, with rare cases of amplification of the gene coding for the FGFR1 tyrosine kinase receptor and rare mutations in kinases such as PI3K or c-KIT (George et al., 2015). Whether these rare events contribute to SCLC development or response to therapy remains poorly understood (Ferone et al., 2020). Little is also known about phosphatases in SCLC beyond inactivation of the gene coding for PTEN (Cui et al., 2014; McFadden et al., 2014).

Here, we surmised that even in the absence of recurrent mutations in genes coding for kinases, SCLC cells may still have active kinases that contribute significantly to the proliferation, survival, and tumorigenic characteristics of SCLC.

RESULTS

A kinome profiling strategy identifies active kinases in SCLC

We used Multiplexed Inhibitor Beads (MIBs) columns to enrich for active kinases in SCLC. Briefly, protein lysates were placed on columns made of sepharose beads bound to ATP-mimic kinase inhibitors. Kinases in an active conformation are bound by the specific inhibitors at the top of the column or by pan-kinase inhibitors at the bottom while inactive kinases flow through (Duncan et al., 2012) (Figure 1A) (see Methods). We compared three SCLC patient-derived xenografts (PDXs) and eight allografts (isolated from an autochthonous mouse model – see below) to non-small cell lung cancer (NSCLC) samples (two adenocarcinoma PDXs, one squamous lung cancer PDX, and four single-tumor derived allografts from a lung adenocarcinoma mouse model driven by oncogenic K-Ras^{G12D}) to avoid enriching solely for kinases activated during the cell cycle. Normal murine lungs were used as an additional control. Unsupervised hierarchical clustering analysis of the mass spectrometry data showed that SCLC and NSCLC samples clustered according to their biological identity (Figure S1A-B). At the intersection of these comparisons, we identified 20 kinases that were more active in SCLC than in normal lungs or NSCLC (Figure 1B-C and Table S1). The 20 kinases have a wide range of mRNA expression levels in human SCLC tumors (Table S1), indicating that the MIBs approach was not biased towards highly expressed proteins. Amongst the top 20 candidates, we identified kinases such as WEE1 and AURKB (Aurora kinase B), which are known to play a role in SCLC (Gay et al., 2019;

Gong et al., 2019; Lallo et al., 2018; Mollaoglu et al., 2017; Oser et al., 2019; Sen et al., 2017a; Sos et al., 2012). We note that the ATP binding sites of other kinases that may play a role in SCLC, such as CHK1, CHK2, ATM and ATR, are not expected to be bound by the inhibitors on the columns (Manning et al., 2002). EPHA5 has been found to be upregulated in SCLC metastases (Wu et al., 2016), but its role in SCLC is not known. Overall, the MIBs approach successfully identified active kinases in SCLC.

PKA is expressed and active in human SCLC

Among the top kinases identified, we decided to focus on protein kinase A (PKA) because of observations in rare human genetic syndromes in which mutations in the PKA pathway lead to the development of neuroendocrine (NE) tumors, including pituitary tumors in people with Carney complex and adrenal tumors in people with Cushing's syndrome (see Discussion). Based on our data and these observations, we surmised that PKA might have a broader role than previously suspected in NE cancers, especially SCLC.

PKA in its inactive form is a tetramer of two catalytic and two regulatory subunits; dissociation of the regulatory subunits upon binding to cyclic AMP (cAMP) results in the activation of the kinase. *PRKACA*, which codes for the catalytic subunit α of PKA (PKA-Cα) identified in the MIBs assays, is the dominant catalytic subunit expressed in SCLC (Figure 1D, Figure S1C, and Table S1). When we analyzed SCLC human tissue microarrays by immunostaining with an antibody recognizing a phosphorylated PKA (pPKA) substrate consensus peptide, we found that 37.5% of the human tumors examined showed positive staining in this assay (Figure 1E). Tissue microarrays probed with an antibody recognizing phosphorylated CREB (pCREB, cAMP Response Binding Element factor 1, CREB), a well-known target of PKA, suggested activation of the PKA/CREB pathway in 17.5% of tumors (Figure S1D). Finally, $Rb1^{flox/flox}$;$Trp53^{flox/flox}$;$Rbl2^{flox/flox}$ conditional mutant mice develop *Rb/Trp53/Rbl2* triple knockout (TKO) SCLC tumors in their lungs upon infection with an adenovirus expressing the Cre recombinase (Ad-Cre) (Gazdar et al., 2015; Schaffer et al., 2010). Immunoblot analysis of TKO SCLC tumors also revealed elevated PKA relative to normal mouse lung (Figure 1F). Thus, PKA is expressed and active in SCLC.

PKA activity is required for the development and the maintenance of SCLC

To investigate the role of PKA activity in SCLC *in vivo*, we crossed TKO mice to a conditional allele of *Prkaca*, whereby expression of Cre results in a switch from wild-type to a mutant form in which a methionine has been replaced by an alanine in the ATP binding site (analog-sensitive, AS, see below – PKA-$C\alpha^{M120A}$). PKA-$C\alpha^{M120A}$ does not utilize endogenous ATP as efficiently as the wild-type enzyme (PKA-$C\alpha^{WT}$) and is thus less catalytically active (Morgan et al., 2008). Switching from PKA-$C\alpha^{WT}$ to PKA-$C\alpha^{M120A}$ at the time of cancer initiation in TKO;$Prkaca^{M120A/M120A}$ mice (Figure S2A-C) led to a significant inhibition of SCLC development compared to control TKO mice (Figure 2A-C). PKA-$C\alpha^{WT}$ and PKA-$C\alpha^{M120A}$ TKO tumors had a similar histology and expressed neuroendocrine markers such as Synaptophysin (SYP) (Figure 2A). We were unable to accurately compare cell proliferation and death in the two groups as the PKA-$C\alpha^{WT}$ tumors were much more advanced than PKA-$C\alpha^{M120A}$ tumors. Expression of PKA-Cα was similar in both models but PKA activity was decreased by ~50% in TKO PKA-$C\alpha^{M120A}$, as would

be expected for this hypomorphic mutation (Figure 2D-F). Thus, a reduction of PKA-Cα activity by half is sufficient to potently inhibit SCLC development in this mouse model.

SCLC cell lines derived from PKA-Cα^{M120A} TKO tumors showed decreased survival in culture compared to TKO cells (Figure S2D). Knockdown of PKA-Cα in KP1 (*Rb1/Trp53* mutant) and KP11 (*Rb1/Trp53/Rbl2* mutant) cell lines also led to decreased growth and increased apoptosis (Figure S2E-H). Similar phenotypes were observed with allografts from KP1 cells (Figure S2I-J). In the Cancer Dependency Map project (DepMap, www.depmap.org), knockdown of PKA-Cα also led to decreased growth in 25 human SCLC cell lines (Figure 2G). Notably, NCI-H526 cells were identified in this analysis as the most dependent on PKA-Cα. Indeed, knockdown of PKA-Cα in these cells led to an increase in apoptosis and a significant inhibition of tumor growth in mice (Figure 2H-J and Figure S2K).

Protein phosphatase 2A (PP2A) counteracts the pro-tumorigenic effects of PKA in SCLC

Previous studies have indicated possible functional interactions between PKA, a serine/threonine protein kinase, and the serine/threonine protein phosphatase PP2A (Ahn et al., 2007; Dodge-Kafka et al., 2010; Musante et al., 2017; Zakany et al., 2002). We found that treatment with the PP2A inhibitor (PP2Ai) cantharidin inhibited PP2A activity (Figure S3A) and enhanced the phosphorylation of PKA substrates in SCLC cells, including VASP (Vasodilator-stimulated phosphoprotein) and CREB (Figure 3A-B). This was prevented by pre-treatment with a PKA inhibitor (PKAi) (Figure 3B), supporting a model in which PP2A activity counteracts PKA activity in SCLC cells. *PPP2R1A* is the most highly expressed PP2A α subunit in human SCLC, and SCLC cells are dependent on *PPP2R1A* expression for their growth in the DepMap dataset (Figure S3B-C). Treatment of SCLC cells with two independent small molecule activators of PP2A (or SMAPs), which act via inhibition of PPP2R1A (Grossman et al., 2017; Kastrinsky et al., 2015; Sangodkar et al., 2017), suppressed PKA substrate phosphorylation and induced apoptosis in SCLC cells (Figure 3C and Figure S3D-E). PP2A has multiple targets in cells, and we found that SMAP treatment also had potent effects on c-MYC expression and mTOR activity in cells (Figure S3F), indicating that PKA signaling inhibition may represent only a fraction of the effects of PP2A activation in SCLC cells. Nevertheless, treatment with the SMAP-1154 tool compound as a single agent led to suppression of tumor growth in NJH29 SCLC xenografts (Figure S3G), with decreased phosphorylation of PKA substrates (Figure S3H). Treatment with a more bioavailable compound (SMAP DT-061) (Sangodkar et al., 2017) had a potent inhibitory effect with induction of apoptosis in a different SCLC xenograft model (NCI-H69 cells) in combination with chemotherapy treatment (cisplatin) (Figure 3D-F and Figure S3I-J). Thus, inhibition of PKA itself or manipulation of other enzymes in the PKA signaling network may have anti-cancer effects in SCLC.

GNAS is genetically activated in human SCLC and promotes PKA activity and SCLC growth in mouse models

PKA is activated in cells in response to increased concentrations of cyclic AMP (cAMP) following conversion of ATP by adenylate cyclase (AC) enzymes. AC and PKA are key mediators of signaling downstream of G protein-coupled receptors (GPCRs). We found Gαs

(encoded by *GNAS)* to be the most highly expressed G-protein α subunits in human SCLC (Figure S4A). Gαs mediates GPCR signaling by activating AC, leading to downstream activation of PKA (Iglesias-Bartolome et al., 2015). In a clinical sequencing cohort of over 300 patients at the Memorial Sloan Kettering Cancer Center, 5 tumors had amplification of *GNAS* and one tumor had a known oncogenic R201C mutation in Gαs (Landis et al., 1989) (Figure S4B). These observations suggested that the PKA pathway may be activated in human SCLC *via* genetic events leading to increased Gαs activity.

To test the role of Gαs in SCLC, we crossed $Gnas^{flox/flox}$ mice to TKO mice (Figure S4C). *Gnas* deletion in this context (Figure S4D) led to decreased tumor development compared to TKO mice (Figure 4A-D), indicating that Gαs is required for optimal cancer initiation in this model. To next determine if Gαs activation could promote SCLC development, we crossed TKO mice to transgenic mice expressing a constitutive active form of Gαs ($Gnas^{R201C}$ allele) following Cre expression and doxycycline (Dox) treatment (Iglesias-Bartolome et al., 2015) (Figure S4E). TKO;$Gnas^{R201C}$ mice developed both SCLC tumors and non-SCLC tumors 3.5 months after Ad-Cre instillation (Figure S4F), indicating that $Gαs^{R201C}$ strongly promotes lung cancer development in this genetic context. Nevertheless, TKO;$Gnas^{R201C}$ mice still developed more and larger SCLC tumors compared to TKO controls, as determined by immunostaining for the neuroendocrine marker synaptophysin (SYP) (Figure S4G-I). Induction of $Gαs^{R201C}$ for 6 weeks (with Dox), 14 weeks after Ad-Cre infection, led to a significant increase in SCLC development, with no growth of large non-SCLC tumors (Figure 4E-H), demonstrating an oncogenic role for $Gαs^{R201C}$ in SCLC progression. In primary cultures derived from TKO;$Gnas^{R201C}$ tumors, expression of $Gαs^{R201C}$ led to an increase in PKA kinase activity and in the phosphorylation of PKA substrates (Figure 4I-J). When we analyzed tumor sections from TKO and TKO;$Gnas^{R201C}$ SCLC tumors, as well as TKO;$Gnas^{flox}$ SCLC tumors, we found no differences in cell death or proliferation associated with changes in Gαs activity (Figure S4J-M). While these counts may be confounded by differences in tumor sizes, these observations suggested that the mechanisms by which activation of PKA potently promotes the development of SCLC *in vivo* may not be as simple as regulation of cell survival and cell division (see below). These experiments demonstrate that amplification and activating mutations in *GNAS* that occur in SCLC patients can significantly enhance SCLC progression in a mouse model, defining Gαs as an oncogene in SCLC.

Identification of a high-confidence proximal PKA signaling network in SCLC cells

We next performed a systems-level proteomic and transcriptomic analysis of PKA in SCLC cells and tumors to identify the proximal PKA pathway and direct kinase substrates, map how the phosphoproteome changes in response to PKA activation, and determine how PKA activation alters the biology of SCLC. First, we sought to identify the PKA interactome in SCLC cells. We expressed LAP-tagged forms (localization and affinity purification tag, LAP-tag) of PKA-Cα, PKA-Cβ, and PKA-R1A in NCI-H446 SCLC cells (Torres et al., 2009) and performed mass spectrometry on the eluted fractions after purification (Figure 5A and Figure S5A). This analysis identified 128 candidate interactors (Table S2). We found complex interactions between catalytic and regulatory PKA subunits, suggesting that loss or inhibition of a single catalytic enzyme may not fully reveal the function of PKA in SCLC

cells (Figure S5B). We compiled a high confidence protein-protein interaction network containing proteins that were identified with at least two baits (Figure 5B). This proximal network contained core components of the PKA pathway such as A-kinase anchoring proteins (AKAPs), PKA catalytic and regulatory subunits, and the cAMP-specific phosphodiesterase 7A (PDE7A), as well as GPR161, a PKA-and cilia-associated protein GPCR (Bachmann et al., 2016; Logue and Scott, 2010; Mukhopadhyay et al., 2013) (Figure 5C). Notably, we found that PKA interacts with SOX2, which is an oncogenic driver in SCLC (Rudin et al., 2012). Furthermore, PKA interacts with PDE4DIP (Phosphodiesterase 4D Interacting Protein), which is recurrently mutated in SCLC (George et al., 2015); inactivating mutations in PDE4DIP may affect PKA signaling directly as an AKAP (Uys et al., 2011) or indirectly by changing the function of PDE4, which is a regulator of cAMP levels (Houslay and Adams, 2003). Together, this analysis further places PKA downstream of GPCR/Gαs signaling networks in SCLC cells and links PKA signaling to additional genetic alterations in primary human SCLC tumors.

Global proteomic analysis of direct PKA substrates and downstream phosphoproteome

When we knocked down the PKA target CREB in murine SCLC cells, we did not observe any inhibition of SCLC cell growth in culture or in mice (Figure S6A-D). These results suggested that PKA promotes SCLC growth largely through other targets. To identify potential direct PKA substrates in SCLC cells, we used the PKA-Cα^{M120A} analog-sensitive (AS) form of PKA. This gatekeeper mutation results in a kinase that cannot efficiently use ATP but instead allows for the incorporation of bulky ATP analogs such as Bn-ATPγS, which are inefficiently used by wild-type kinases and can serve to identify direct kinase substrates following the covalent capture of thiophosphorylated peptides (Hertz et al., 2010) (Figure 6A). We selected two PDX models (NJH29 and LX102), one allograft model (derived from a TKO mouse, 5BI), and one human cell line (NCI-H82), which are representative of the diversity of molecular phenotypes in human SCLC (Rudin et al., 2019) (Figure S6E). As expected, recombinant active PKA (rPKA) was better able to phosphorylate substrates with ATP while rAS-PKA (PKA-Cα^{M120A}) was better at using Bn-ATPγS (Figure 6B-C and Figure S6F-G). Large-scale labeling reactions were performed, and mass spectrometry identified ~200 substrates that were labeled by rAS-PKA but not by wild-type rPKA (Table S3). Because there was little overlap in the identity of the substrates between the different tumors used, and because known substrates such as CREB and VASP were not found in this analysis, this number of substrates likely underestimates the total number of PKA substrates in SCLC cells. Among the identified substrates, at least 31 have been described before (Baba et al., 2011; Imamura et al., 2014; Isobe et al., 2017; Moore et al., 2009; Nagai et al., 2016) (Table S3). The majority of substrates had the canonical PKA motif RXXS/T (Figure 6D). GO term analysis showed enrichment in multiple signaling pathways involved in cell cycle, gene expression and metabolic processes (Figure 6E). Together, these data indicate that PKA phosphorylates hundreds of substrates in SCLC and identify a broad role for PKA in cell cycle and cell growth mechanisms that can promote SCLC expansion.

To gain further insight into the downstream consequences of PKA activation in SCLC cells, we next performed a global phosphoproteomic analysis in NCI-H526 cells (highly

dependent on PKA activity, Figure 2G-I) and NCI-H69 cells (which have relatively high PKA activity, Figure S6H). Upon PKA activation with a long-acting analog of cAMP (8-Br-cAMP) (Figure 6F), we identified thousands of phosphorylation sites, both gains and losses, which changed in response to 8-Br-cAMP (Tables S4). The functional significance of the changes in phosphorylation that we observed upon PKA activation remains unknown for nearly all the proteins analyzed. However, GO term analysis for the phosphoproteome affected by cAMP in both cell lines showed enrichment for a variety of pathways implicated in cell proliferation and cancer (Tables S4, Figure 6G, and Figure S6I), similar to the pathways enriched in the AS-PKA experiments. 54 PKA substrates identified using the AS-PKA approach were also identified using the global phosphoproteomic approach (Table S5). Knockdown of some of these high-confidence targets, including ribosome subunits (RPL34, RPS3A, RPS6), decreases the growth of human SCLC cell lines in the DepMap dataset (Figure 6H). This multifaceted approach identified a large number of substrates for PKA, and the results of this analysis indicate that PKA activation promotes SCLC growth by regulating multiple signaling networks.

PKA activity promotes a cancer stem cell state in SCLC

To investigate the cellular consequences of PKA activation in SCLC cells, we expressed a doxycycline-inducible version of PKA-Cα with reduced capability for inhibition by regulatory subunits (active PKA, or aPKA) (Orellana and McKnight, 1992) or a GFP control in human NCI-H82 and NJH29 SCLC cells, which have relatively low PKA activity when compared to other SCLC cell lines (Figure S6H). Expression of aPKA led to a moderate increase in PKA signaling and a significant increase in the growth of xenografts (Figure 7A and Figure S7A-D). We performed RNA-seq of these xenografts (Table S6). PANTHER pathway analysis on the genes downregulated in both models ($P<0.05$) revealed changes in various signaling pathways, including cell adhesion and cell death (Figure S7E). Analysis of the upregulated genes in aPKA-expressing tumors revealed pathways associated with neuronal and neuroendocrine features (Figure S7F). In particular, we noticed a significant up-regulation of a number of markers of SCLC cancer stem cells (Jahchan et al., 2016), including *NCAM1, DLL3, MYCL*, and *CD24* (Table S6, Figure 7B and Figure S7G-H). This connection between PKA activation and cancer stem cell phenotypes was supported by the interaction between PKA and SOX2 (Figure 5B), which is a known regulator of stem cells (Novak et al., 2019), as well as the identification of the histone demethylase PHF2 as a direct PKA substrate (Table S3), PHF2 having been implicated in the expansion of breast cancer stem cells (Pattabiraman et al., 2016).

These observations led us to test the possibility that a key output of PKA is the promotion of cancer stem cell phenotypes in SCLC. We tested this idea in two human tumor model systems. First, as we observed an increase in tumor growth and upregulation of cancer stem cell markers such as CD24 (Jahchan et al., 2016) or DLL3 (Saunders et al., 2015) in NJH29 xenografts upon PKA activation (Figure 7A), we performed an extreme limiting dilution analysis (ELDA) by transplanting dilutions of NJH29-GFP and NJH29-aPKA cells into NSG mice. Activation of PKA was sufficient to enhance the frequency of SCLC cancer stem cells in this context (Figure 7C). Conversely, knockdown of PKA-Cα in NCI-H526 cells, which are dependent on PKA activity (Figure 2G-I), decreased expression of cancer stem

cell markers (Figure 7D-E) and decreased the frequency of tumor-initiating cells (Figure 7F). The expression of cancer stem cell markers was also significantly reduced in the resulting tumors (Figure 7G). Thus, alterations in PKA activity in SCLC cells results in changes in signaling networks that control gene expression programs governing the cancer stem cell state.

DISCUSSION

SCLC is one of the most fatal forms of cancer. In contrast to many other cancer types, DNA and RNA sequencing of SCLC tumors have identified few actionable therapeutic targets that may apply to a large number of patients. Using a proteomics approach, we identified 20 candidate kinases that are more active in SCLC cells than in normal lungs or NSCLC cells. Among these kinases, we confirmed that PKA is active in a large fraction of SCLC cases, and that PKA activity is required for the optimal growth of SCLC tumors.

A striking association exists between PKA activity and endocrine and neuroendocrine tumors. First, activating mutations in *PRKACA* were identified in Cushing's syndrome, which includes abnormal growth of endocrine cells in the adrenal gland (Beuschlein et al., 2014; Cao et al., 2014; Goh et al., 2014; Kirschner, 2014; Sato et al., 2014). Second, inactivating mutations in a regulatory subunit of PKA (*PRKAR1A* gene) in Carney complex are associated with the development of tumors from endocrine tissues such as the pituitary gland (Horvath et al., 2010; Kirschner et al., 2000). Third, somatic activating mutations in *GNAS* in McCune-Albright syndrome result in multiple endocrine neoplasia (Salpea and Stratakis, 2014; Weinstein et al., 1991). Finally, increased expression of PKA-Cα from a *DNAJB1-PRKACA* fusion leads to the development of fibrolamellar hepatocellular carcinoma, a rare form of liver cancer with neuroendocrine features (Honeyman et al., 2014; Xu et al., 2015). In mice, knockout of *Prkar1a* initiates neuroendocrine cancer in the pancreas (Saloustros et al., 2017). These data indicate that PKA may act as an oncogene in the initiation of infrequent neuroendocrine cancers. A study with a dominant-negative form of PKA suggested that PKA might also be important in SCLC cells (Xia et al., 2018). Similarly, loss of *Prkar1a* was found to promote the growth of SCLC cells in culture (Li et al., 2019). Our work extends these observations and conclusively demonstrates in multiple contexts that PKA kinase activity is critical for the development and the maintenance of SCLC, the most common and lethal form of neuroendocrine cancer.

How is PKA activated in SCLC cells? Recurrent alterations in genes such as *GNAS* or *PDE4DIP* may lead to PKA activation in 5-10% of SCLC cases, and it is possible that other recurrent genetic events contribute to activation of PKA signaling, including mutations in GPCRs upstream of Gαs and PKA (Rudin et al., 2012). A genomic region encompassing *Gnas* is amplified in mouse SCLC tumors (McFadden et al., 2014), and we speculate that *Gnas* in this amplicon is the driver of this chromosomal alteration. A number of GPCRs are expressed and active in SCLC cells (Teicher, 2014). We previously showed that SCLC cells may activate these GPCRs via autocrine mechanisms and that the simultaneous inhibition of several of these GPCRs with imipramine, a tri-cyclic antidepressant, could inhibit the growth of SCLC, which correlated with decreased PKA activity (Jahchan et al., 2013). We note that imipramine may also directly activate PP2A, which may have contributed to its anti-cancer

activity (Kastrinsky et al., 2015). Based on our RNA-seq data that activation of PKA can result in the increased expression of genes coding for GPCRs (e.g. *DRD2, CHRM4*, or *GRM2*), these autocrine/paracrine loops may be maintained by constant positive feedback, thereby sustaining high PKA activity in SCLC cells, even in the absence of genetic alterations in this pathway.

Why PKA is oncogenic in neuroendocrine tumors but tumor-suppressive in some other contexts is not completely elucidated, but our work suggests a possible model. PKA activation correlates with a more epithelial, more neuroendocrine state in SCLC cells, a state that we and others previously found was associated with increased tumorigenicity (Augustyn et al., 2014; Borromeo et al., 2016; Jahchan et al., 2016). Similarly, PKA activation is sufficient to reprogram hepatocytes towards a more neuroendocrine state in fibrolamellar hepatocellular carcinoma (Kastenhuber et al., 2017) and for the acquisition of neuroendocrine-like features in prostate cancer (Deeble et al., 2007). Interestingly, in breast cancer cells, PKA activation promotes a mesenchymal-to-epithelial (MET) transition associated with decreased tumorigenicity (Pattabiraman et al., 2016). Therefore, PKA may generally promote a more epithelial state in cancer cells, but this state may correspond to less aggressive cancer cells in cancers where loss of epithelial features accompanies tumor progression, and more aggressive cancer cells in neuroendocrine cancer where tumor-propagating cells are more epithelial.

PKA is ubiquitously expressed and essential for many cellular processes, including embryonic development (Skalhegg et al., 2002). However, our data showing that a 50% decrease in PKA activity is sufficient to significantly inhibit tumor growth in mice suggest that there may be a therapeutic window for PKA inhibitors, especially in combination with other agents. Whether specific and potent PKA inhibitors may one day be available to treat cancer patients is unknown, but an alternative pathway to inhibit PKA in SCLC and other neuroendocrine cancers may be through activation of PP2A, which dephosphorylates PKA substrates and has other tumor suppressive effects (Mazhar et al., 2019). While PKA inhibitors and PP2A activators need to be further developed and tested in pre-clinical models, our efforts highlight the possibility of targeting this signaling axis to thwart SCLC progression. Importantly, our work underscores the possibility of targeting non-mutated, ubiquitous signaling pathways to treat specific cancer types such as SCLC, and raises the possibility that genetic alterations in these pathways might help identify patients most responsive to these therapeutic strategies.

STAR METHODS

RESOURCE AVAILABILITY

LEAD CONTACT—Information regarding the request of materials and reagents should be directed to and will be fulfilled by the lead contact and corresponding author, Julien Sage (julsage@stanford.edu).

MATERIALS AVAILABILITY—Plasmids generated in this study are available upon request. Please email the lead contact and corresponding author, Julien Sage (julsage@stanford.edu) for requests.

DATA AND CODE AVAILABILITY—The proteomics datasets generated in this study are available at ProteomeXChange, accession numbers PXD018209 and PXD017704, http://www.proteomexchange.org/.

The RNA sequencing datasets generated in this study are available at GEO, accession number GSE126353, https://www.ncbi.nlm.nih.gov/geo/.

EXPERIMENTAL MODELS AND SUBJECT DETAILS

Mouse models—All experiments regarding the use of mice were performed per protocols set in place by the National Institute of Health at Stanford's Research animal facility or the University of Michigan. All treatments were performed un-blinded, but all measurements and quantification were performed in a blinded fashion. The generation and initiating of SCLC tumors in TKO mice with conditional alleles of *Rb1*), *Trp53*, and *Rbl2* were performed as previously described (Schaffer et al., 2010). TKO mice are maintained on a mixed C57BL/6;129/SVJ background and tumors cells from these mice can be engrafted in B6129SF1/J hybrid (F1) mice (JAX # 101043).

To examine the role for *Prkaca* in SCLC lung tumors, $Prkaca^{M120A}$ mice were crossed to TKO mice. Mice were genotyped as previously described (Morgan et al., 2008). Tumors were initiated by intratracheal administration $4x10^7$ plaque-forming units of Adeno-CMV-Cre (University of Iowa) into 10-week-old mice and animals were collected 5 months later. The lungs were fixed, the heart and connective tissue removed, the lungs were weighed before processing for histology. H&E-stained sections were imaged on a Keyence microscope and tumor number and tumor area were quantified in image J as previously described (Lim et al., 2017).

To determine the requirement for *Gnas* in SCLC, we crossed $Gnas^{flox/flox}$ mice (Chen et al., 2005) to TKO mice. We then crossed TKO;$Gnas^{flox/+}$ mice to generate TKO;$Gnas^{flox/flox}$ and littermate controls. Mice were genotyped as described in (Iglesias-Bartolome et al., 2015). Tumors were initiated as described above.

To examine the consequences of Gαs activation in SCLC, we used a Cre- and doxycycline-inducible $GNAS^{R201C}$ model with $Rosa26R^{LSL\text{-}rtTA}$ (B6.Cg-$Gt(ROSA)26Sor^{tm1(rtTA,EGFP)Nagy}$/J, The Jackson Laboratory 005670) and TetO7-$GNAS^{R201C}$ mice (Iglesias-Bartolome et al., 2015) that we crossed to TKO mice. In this model, delivery of the Cre recombinase in lung epithelial cells results in the deletion of the three tumor suppressor genes and removal of a stop cassette upstream of a reverse tetracycline transactivator (rtTA). In the presence of doxycycline, binding of rtTA to the Tet operon (TetO) upstream of $GNAS^{R201C}$ in the same transgene results in expression of an active form of Gαs.

For allografts, individual SCLC tumors were micro dissected from TKO mice, single cell suspensions were generated (see below) and $1.0x10^6$ live cells were injected into the flanks of F1 mice. Cells were mixed with 50% Matrigel (BD Biosciences) and media with 10% serum but lacking antibiotics. For *Prkaca* knockdown studies, KP1 cells were injected into the flanks NOD.Cg-$Prkdc^{scid}IL2rg^{tm1Wjl}$/SzJ (NSG) mice. KP1 were described in (Park et

al., 2011)). Lung adenocarcinoma allografts were grown from cell lines derived from *Kras/Trp53* lung tumors (K-Ras^{G12D} and p53 null (Zheng et al., 2013)); these cell lines were a gift from Leanne Sayles and Dr. Alejandro Sweet-Cordero.

Patient-derived xenograft models—For xenograft studies, 1.0 - 2.0x10^6 cells were injected into the flanks of NSG mice with 1:1 mixture of Matrigel and antibiotic-free media. The PDX SCLC models used in this report were NJH29 (Jahchan et al., 2013), JHU-LX102 (Leong et al., 2014) (a gift from Dr. Neil Watkins), and JHU-LX92 (Poirier et al., 2015) (a gift from Dr. John Poirier and Dr. Charles Rudin). The NSCLC PDX models used were JHU-LX55a ((Manchado et al., 2016) (a gift from Dr. John Poirier and Dr. Charles Rudin), PDX727 and PDX0131 (a gift from Leanne Sayles and Dr. Alejandro Sweet-Cordero). For the doxycycline-inducible aPKA vector (or GFP control), 1.8 g doxycycline (Sigma) and 9 g of sucrose were added to 900 mL of water and provided to mice approximately 3 days after tumor initiation. The water was changed weekly. Subcutaneous tumor volume was quantified by measuring the length and width of tumors using a digital caliper and the volume was determined as previously described (Jahchan et al., 2013).

Mice bearing SCLC tumors were randomized before treatment and treated once/day with 50 mg/kg JNS-1-40 by I.P. injections (Grossman et al., 2017), twice daily with SMAP-1154 (100 mg/kg) or 5 mg/kg SMAP-DT-061 by oral gavage (Sangodkar et al., 2017). 4 mg/kg cisplatin (Mount Sinai Hospital pharmacy) was administered to mice once per week by I.P. injections.

For limiting dilution analyses, ELDA software, which uses the frequency of tumor-positive and negative injections at each transplant dose (Hu and Smyth, 2009), was used to determine the frequency of cancer stem cells (http://bioinf.wehi.edu.au/software/elda/). P values comparing groups were calculated as before (Jahchan et al., 2016).

Cell culture—KP1 (*Rb1/Trp53* mutant, DKO), and KP11 (*Rb1/Rbl2/Trp53* mutant, TKO) mouse SCLC cells were generated from single tumors (Park et al., 2011). Allografts tested in the multiplexed inhibitor beads inhibitors assays were derived from single tumors. NJH29 cells were previously generated in our laboratory from a PDX model (Jahchan et al., 2013), and A549, NCI-H69, NCI-H82, NCI-H187, and NCI-H446 were purchased from ATCC. Cells were grown in RPM1-1640 media supplemented with 10% bovine growth serum (BGS, Fisher Scientific) and penicillin-streptomycin–glutamine (PSQ, Gibco). Cells were grown at 37C in standard cell culture incubators. All cell lines are routinely tested (Lonza) and confirmed to be free of mycoplasma contamination.

METHOD DETAILS

PKA/PP2A stimulation and inhibition—For stimulation or inhibition of endogenous PKA and PP2A, SCLC cells were plated overnight in media containing 2% BGS. The following day 100 μM 8-Br-cAMP (Tocris), 20 μM H89 (Tocris), 10 μM cantharidin (Tocris), or 10 μM SMAP-1154 were added to cells in media containing 2% BGS for 60 min or as described in the figure legends. The *Prkaca* knockdown studies, all cell viability assays, and immunoblots/immunoassays were also performed in media containing 2% BGS.

Single cell suspension—To generate single cell suspensions and to isolate primary tumor cells for in vitro assays, TKO control and *Prkaca*^{M120A} mutant SCLC tumors were collected from mice at ~6 months following tumor initiation and tumor tissue was digested with Collagenase/Dispase (Roche) as described by (Jahchan et al., 2016). Cells were plated in 6 well plates and SCLC cells growing in suspension were selected for so that after 6 passages cultures were depleted of contaminating stromal cells. Tumor cells were genotyped using standard methods. All SCLC cells isolated from both control and PKA-Cα^{M120A}-mutant tumors had undergone recombination in the conditional alleles. Cells were then used in cell viability and kinase assays.

Cell viability assays—Either $8x10^3$ human or 10^4 mouse SCLC suspension cells were plated in flat bottom 96 well plates in 200 μL of media containing 2% BGS and plates were incubated for 2-6 days before AlamarBlue (Thermo Fisher Scientific) reagent was added and plates were read after 2 hours according to manufactures specifications. Plates were not re-fed.

RNA purification, RT-qPCR, and RNA sequencing—Frozen tumor samples were ground with a mortar and pestle and total RNA was extracted using the RNeasy Mini Kit (Qiagen). For RT-qPCR, 1 μg of total RNA was used to make cDNA using the NEB ProtoScript cDNA synthesis kit, and cDNA was diluted 1:20 before use. Gene specific RT-qPCR primers for mouse Gnas were described in Chen et al., 2005 (Table S7). The remaining gene specific RT-qPCR primers were obtained from the Mass General Primer Bank and are described in (Table S7).

For RNA-seq analysis, 2 μg of total RNA was used to prepare cDNA libraries with the TruSeq Stranded Total RNA LT Kit (Illumina). Libraries were sequenced at the Stanford Functional Genomics Facility using a NextSeq sequencing system. Reads were mapped to human reference genome hg19 with STAR2.5.1b using default settings. Genes that have at least ten reads in three out of six samples in one condition were used for further analysis. Differentially expressed genes were obtained using DEseq2. Panther pathway analysis was performed using the Enrichr platform (Chen et al., 2013). The accession number for the RNA-Seq results is GEO: GSE126353.

Immunoblot analysis, Immunoassays, and Immunostaining—Cells or tumors were lysed and sonicated in RIPA lysis buffer (Pierce) with protease and phosphatase inhibitor tablets (Roche). Protein concentration was measured using the Pierce BCA Protein Assay Kit (Thermo Fisher Scientific) and 10 μg of protein was analyzed by immunoblot. For immunoassays, 1 μg of protein was analyzed using the Simple Western quantitative immunoassay and the Compass software, according to the manufacturer's protocol. Immunoblots were quantified in Image J and target proteins were normalized to loading control for each sample.

Tumor samples were fixed in 4% formalin and embedded in paraffin before staining with hematoxylin and eosin or immunostaining (immunohistochemistry), as previously described. (Lim et al., 2017) Images were quantified using ImageJ. Tissue microarrays were stained and scored by a board-certified pathologist, C.S. Kong.

TUNEL staining was performed as previously described using the ApopTag Fluorescein In Situ Apoptosis Detection Kit (Millipore) according to the manufacturer's protocol (Sangodkar et al., 2017). DAPI was used to counterstain the DNA.

In vitro kinase and phosphatase assays—For testing the kinase activity of endogenous PKA-Cα in TKO and TKO;*Prkaca*^{M120A} SCLC tumor cells, cells were lysed and sonicated in cell lysis buffer (CST# 9803) with protease and phosphatase inhibitor tablets (Roche). 1 mg of extract was incubated with 10 μL of PKA-Cα antibody (CST# 4782) or normal rabbit IgG (CST #2729) overnight with gentle rotation. The following day 50 μL pre-washed protein A-agarose beads (Sigma #P3476) were added and incubated at 4°C for 60 min with gentle shaking. Beads were washed then incubated with 20 μg of NJH29 PDX native tumor cell extract (isolated with CST #9803), ATP (CST #9804), and 1X kinase buffer (CST # 9804, 9802) at 37°C for 60 min. Samples were then incubated with 6X Laemmli buffer and analyzed by immunoblot using the phospho-PKA substrate antibody (CST# 9624). Signal intensity was measured using Image J software and normalized to PKA-Cα expression. For testing the kinase activity of recombinant enzymes 1 μg of recombinant rPKA or rAS-PKA (M120A mutant) was used in the kinase assays.

Total cellular PKA kinase and PP2A phosphatase activity was measured using commercially available kits (PKA Colorimetric Activity Kit, Thermo Fisher Scientific; PP2A Immunoprecipitation Phosphatase Assay Kit, Millipore) according to the manufacturers' instructions.

Purification of recombinant enzymes—The PDK1-PKA co-expression system was used to purify active recombinant rPKA and rAS-PKA as previously described (Schauble et al., 2007). The PKA-Cα^{M120A} expression vector was generated by synthesizing a fragment containing the M120A mutation that was flanked between *Nde*1 and *Hind*III digest sites. The fragment was then digested and gel purified and ligated into Pet15B. Vectors for His-PKA-Cα and GST-PDK1 or His- PKA-Cα^{M120A} and GST-PDK1 were then co-transformed into BL21 bacteria and placed on 1mM ITPG to induce expression. His-tagged proteins were then purified using Ni-NTA beads (Thermo Fisher Scientific) and immunoblots confirmed that GST-PDK1 did not co-purify with PKA.

Kinome Profiling Sample Processing—Allografts and PDX samples were ground into a fine powder using a mortar and pestle and continuously kept frozen with liquid nitrogen. Powder was then gathered into microcentrifuge tubes, on ice, in 1 mL of lysis buffer (50 mM HEPES pH 7.5, 150 mM NaCl, 0.5% Triton X-100, 1 mM EDTA, 1mM EGTA) with Roche PhosSTOP and Complete Protease Inhibitor tablets added as manufacturer instructs (Sigma-Aldrich). After vortexing lightly, lysates were incubated on ice for 20 min, and re-vortexed lightly every 10 min. Lysates were centrifuged twice at 13,000 RPM for 10 min at 4°C in a tabletop microcentrifuge, and supernatant was removed. Protein concentration was measured by Bradford reagent (CWA #100514-184), and samples were snap-frozen in liquid nitrogen.

Multiplexed Inhibitor Beads (MIBs) assays—Kinase chromatography, mass spectrometry and analytical processing were performed as described previously (Roskoski, 2016; Sos et al., 2014). Bait compounds were purchased or synthesized as described

previously (Sos et al., 2014) and coupled to sepharose using 1-Ethyl-3-(3-dimethylaminopropyl)carbodiimide chemistry. Cell lysates were diluted in binding buffer with 1 mol/L NaCl, and affinity purification was performed with gravity chromatography after pre-clearing. The bound kinases were stringently washed and then eluted with SDS followed by extraction/precipitation, tryptic digest and desalting. Liquid chromatography-tandem mass spectrometry (LC/MS-MS) was performed on a Velos Orbitrap (Thermo Fisher Scientific) with in-line high-performance liquid chromatography (HPLC) using an EASY-spray column (Thermo Fisher Scientific). Label-free quantification was performed with Skyline (Schilling et al., 2012), and statistical analysis with MSstats (Choi et al., 2014).

Covalent Capture—Labeling experiments for covalent capture enrichment were performed on 2 mg of protein lysate per sample (n=2/line) as previously described (Levin et al., 2016). Briefly, samples were incubated in lysis buffer supplemented with 250 μM Bn-ATPγS, 250 μM ATP, 5 mM GTP, 10 mM MgCl2, and 20 μg of purified PKA as indicated. Labeling reactions were performed at 37°C for 60 min before quenching with 50 mM EDTA. Thirty-microliter aliquots of each reaction were alkylated with 2 μL of 100 mM p-nitro mesylate (PNBM) for 30 min at room temperature. Thiophosporylation was detected by immunoblot with the antithiophosphate ester antibody (110C).

Covalent capture of thiophosphorylated proteins was performed as described previously (Hertz et al., 2010). Briefly, lysates were denatured by adding 60% (wt/vol) solid urea, 10 mM final TCEP, and incubating at 55 °C for 30 min. Samples were diluted to 2 M urea with 50 mM ammonium bicarbonate, brought to a pH of 8, and digested overnight at 37 °C with trypsin (Promega) at a 1:20 ratio. Peptides were acidified with trifluoroacetic acid, desalted on a SepPak C18 column (Waters), and speed-vacuumed to dryness. Peptides were resuspended in 50 mM HEPES and 50% (vol/vol) acetonitrile and adjusted to pH 7. The peptide solution was incubated overnight rocking with 100 μL of iodoacetyl Sepharose resin in the dark (Thermo Fisher Scientific). Beads were washed by gravity flow with water, 5 M NaCl, 50% (vol/vol) acetonitrile, 5% (vol/vol) formic acid, and 10 mM DTT followed by elution with 1 mg/mL oxone (Sigma). Peptides were desalted with ZipTips (Millipore) and speed-vacuumed until dry.

LC-MS/MS Analysis and Data Processing—All desalted peptides were resuspended into 10 μL of 0.1% formic acid. Peptides were loaded on to a nanoACQUITY (Waters) UPLC instrument for reversed-phase chromatography with a C18 column (BEH130, 1.7-μm bead size, 100 μm × 100 mm) in front of an LTQ Orbitrap Velos. The LC was operated at a 600-nL/min flow rate and peptides were separated over an 80-min gradient from 2 to 50% buffer B (buffer A: water and 0.1% formic acid; buffer B: acetonitrile and 0.1% formic acid). Survey scans were recorded over a 350–1,800 m/z range and MS/MS fragmentation was performed using HCD on the top eight peaks. A second injection (i.e., technical replicate) of each sample was performed using ETD fragmentation on the top six peaks. Peak lists were generated with an in-house software called PAVA and searched against the SwissProt Homo sapiens database (downloaded June 27, 2013; 20,264 entries) using Protein Prospector (v5.10.10). Data were searched with a 20-ppm tolerance for parent and fragment ions (HCD or 20 ppm/0.6 Da ETD), allowing for standard variable modifications and S/T/Y

phosphorylation. Filtering of background peptides and phosphopeptides was accomplished using an in-house R script described previously (Lipp et al., 2015). The AS-PKA logo motif was generated using the Berkley Berkeley's WebLogo generator (Crooks et al., 2004).

Global Phosphoproteomics—Cells were plated in media containing 2% BGS (described above) and the following day cells treated with vehicle or 8-Br-cAMP for 60 min. Cells were then collected, lysed, and subjected to tryptic digest. Samples were desalted and lyophilized, and phosphoenrichment was performed with immobilized metal affinity chromatography following established protocols (Swaney and Villen, 2016). Phosphopeptides were then additionally desalted and data acquired using a Thermo Q Exactive (Thermo Fisher Scientific). Mass spectrometry was performed at the Thermo Fisher Scientific Proteomics Facility for Disease Target Discovery at UCSF and the J. David Gladstone Institutes. Prospector was used for peptide assignment (http://prospector.ucsf.edu/prospector/mshome.htm) and Skyline was used for all quantification (https://skyline.ms/project/home/software/Skyline/begin.view). Statistical comparison was done using MS Stats (Choi et al., 2014). All gene ontology networks were generated using ClueGO version 2.5.3 through Cytoscape 3.7. Biological Process terms were identified for each group of proteins (phosphorylated, de-phosphorylated, both phosphorylated and de-phosphorylated and direct hits). We used GO Tree Interval min:2 max:5, 8 minimal genes per GO term, kappa score of 0.45 and GO Term fusion. Only p values below 0.05 are displayed.

GO term enrichment analysis was performed on top hits using Metascape with the default settings in the “Express Analysis” function in August 2019 (Zhou et al., 2019).

DepMap analysis—To determine which PKA substrates play key roles in regulating SCLC cell proliferation or survival, we examined dependency scores associated with each gene using the data available from Cancer Dependency Map portal (https://depmap.org/portal/download/) (McFarland et al., 2018). Gene dependency scores were derived from DEMETER2 algorithm applied to combined RNAi screen data (Marcotte et al., 2016). A negative gene dependency score corresponds to greater gene essentiality, such that median gene dependency score of pan-essential genes is normalized to −1 and that of negative control genes is set to 0. We analyzed the distribution of dependency scores from SCLC cell lines (n = 25) for downstream substrate (n = 48 – some of the genes in the common list of candidate targets were not screened by RNAi in DepMap). Genes were organized in an ascending order by median gene dependency scores.

Tandem affinity purification and mass spectrometry—The lentiviral backbone vector (pWPXLd/LAP-N/puro/DEST) vector was created by inserting EGFP-TEV cleavage site-S tag-PreScission cleavage site/DEST/puromycin resistance cassette of pG-LAP6/puro vector into pWPXLd vector, a gift from Prof. Didier Trono (Addgene plasmid #12258). pDONR223-PRKACA-WT was a gift from Jesse Boehm & William Hahn & David Root (Addgene plasmid # 82311). pDONR221-PRKACB (HsCD00296755) and pENTR221-PRKAR1A (HsCD00043858) were obtained from Harvard PlasmID. These vectors were transduced into NCI-H446 human SCLC cells using standard techniques. Tandem affinity purification and analysis were performed as previously described (Kanie et al., 2017; Li et al., 2017). The proteomics data have been deposited to the ProteomeXchange Consortium

via the PRIDE (Vizcaino et al., 2016) partner repository with the dataset identifier PXD017704 and 10.6019/PXD017704.

Large scale synthesis of JNS-1-40—*N*-benzyl-2-chloro-*N*-(2,3-dihydrobenzo[*b*][1,4]dioxin-6-yl)acetamide (JNS-1-40) (Figure S3E, left panel): To a round bottom flask charged with a stir bar and 4 Å molecular sieves was added 1,4-Benzodioxan-6-amine (2.267 g, 15 mmol, 1.5 equiv.). The flask was then put under vacuum and back-filled with nitrogen, and dry DCM (20 mL) was added. To the resulting brown solution was added benzaldehyde (1.02 mL, 10 mmol, 1 equiv.). After 20 min of stirring solid sodium triacetoxyborohydride (3.179 g, 15 mmol, 1.5 equiv.) was added to the flask and the reaction was allowed to progress overnight at room temperature. The resulting reaction mixture was diluted to a total volume of 75 mL DCM and partitioned with 125 mL H_2O. The aqueous layer was back-extracted with 2x 50 mL DCM and the combined organic was washed 1x 100mL $NaHCO_2$ and 1x 100mL brine, before being dried over $MgSO_4$ and concentrated *in vacuo*. The resulting dark brown crude was purified by column chromatography (15% EtOAc:hexane) to afforded SI-1 (2.28 g, 94%) as a yellow oil.

The resulting product was transferred to a stir bar-charged flask and dissolved in 10 mL of dry DCM. Triethylamine (1.9 mL, 13.65 mmol, 1.5 equiv.) was added to the stirring solution. After putting the reaction on ice, chloroacetyl chloride (0.95 mL, 11.96 mmol, 1,3 equiv.) was gradually adding to the stirring mixture. The reaction was allowed to warn to room temperature overnight. The reaction mixture was diluted to a total volume of 50 mL DCM and partitioned with 50 mL saturated $NaHCO_3$. The aqueous layer was back extracted with and additional 50mL DCM and the combined organic layers were washed 1x with 50mL brine and dried over $MgSO_4$. The crude product was concentrated *in vacuo* and purified by column chromatography (30% EtOAc:hexane) to afford JNS-1-40 (2.57 g, 89%) as a yellow wax. Yield over the two-step reaction was 2.57 g, 84%. The product was analyzed by Nuclear magnetic resonance (NMR) (Figure S3E, right panels).

QUANTIFICATION AND STATISTICAL ANALYSIS

Statistical significance was assayed with GraphPad Prism software. Data are represented as mean ± SEM. Unpaired t-tests were performed with all individual data points from all the biological replicates. If F-test (for variance) reported a significantly different distribution between the test groups (F-test $P < 0.05$), the nonparametric Mann–Whitney p value is reported.

Supplementary Material

Refer to Web version on PubMed Central for supplementary material.

ACKNOWLEDGMENTS

We thank Pauline Chu from the Stanford Histology Service Center, Alyssa Ray for her help with figures, Thuyen Nguyen for her help with mice, Drs. Sweet-Cordero, Watkins, Poirier, and Rudin for the allograft and xenograft models, Dr. Winslow for critical reading of the manuscript, and all the members of the Sage lab for their help throughout this study. We thank Dr. Rudin for providing access to the unpublished SCLC cBioPortal data (NCI 1U24CA213274). We thank the UCSF/Gladstone Institute Thermo Fisher Scientific Proteomics Facility for Disease Target Discovery. Research reported in this publication was supported by the American Cancer Society (ACS)

postdoctoral fellowship (G.L.C. and J.G.), the Department of Defense (grant W81XWH-15-1-0250 to Ju.S. and K.S), the Emerson Collective (Ju.S.), the Ludwig Cancer Research foundation (Ju.S.), the Burroughs Wellcome Fund Career award (J.G.), the NSF (GRFP award to S.C. and S.M.M.), the NIH (grant 1S10OD016229-0 to the UCSF shared instrumentation program, grant CA181654 to G.N., grant ES028096 to D.K.N., grants CA201513 and 4CA217450 to Ju.S.), and the Howard Hughes Medical Institute (K.S.). Ju.S. is the Harriet and Mary Zelencik Scientist in Children's Cancer and Blood Diseases.

REFERENCES

Ahn JH, McAvoy T, Rakhilin SV, Nishi A, Greengard P, and Nairn AC (2007). Protein kinase A activates protein phosphatase 2A by phosphorylation of the B56delta subunit. Proc Natl Acad Sci U S A 104, 2979–2984. [PubMed: 17301223]

Augustyn A, Borromeo M, Wang T, Fujimoto J, Shao C, Dospoy PD, Lee V, Tan C, Sullivan JP, Larsen JE, et al. (2014). ASCL1 is a lineage oncogene providing therapeutic targets for high-grade neuroendocrine lung cancers. Proc Natl Acad Sci U S A 111, 14788–14793. [PubMed: 25267614]

Baba A, Ohtake F, Okuno Y, Yokota K, Okada M, Imai Y, Ni M, Meyer CA, Igarashi K, Kanno J, et al. (2011). PKA-dependent regulation of the histone lysine demethylase complex PHF2-ARID5B. Nat Cell Biol 13, 668–675. [PubMed: 21532585]

Bachmann VA, Mayrhofer JE, Ilouz R, Tschaikner P, Raffeiner P, Rock R, Courcelles M, Apelt F, Lu TW, Baillie GS, et al. (2016). Gpr161 anchoring of PKA consolidates GPCR and cAMP signaling. Proc Natl Acad Sci U S A 113, 7786–7791. [PubMed: 27357676]

Beuschlein F, Fassnacht M, Assie G, Calebiro D, Stratakis CA, Osswald A, Ronchi CL, Wieland T, Sbiera S, Faucz FR, et al. (2014). Constitutive activation of PKA catalytic subunit in adrenal Cushing's syndrome. N Engl J Med 370, 1019–1028. [PubMed: 24571724]

Bindea G, Mlecnik B, Hackl H, Charoentong P, Tosolini M, Kirilovsky A, Fridman WH, Pages F, Trajanoski Z, and Galon J (2009). ClueGO: a Cytoscape plug-in to decipher functionally grouped gene ontology and pathway annotation networks. Bioinformatics 25, 1091–1093. [PubMed: 19237447]

Borromeo MD, Savage TK, Kollipara RK, He M, Augustyn A, Osborne JK, Girard L, Minna JD, Gazdar AF, Cobb MH, and Johnson JE (2016). ASCL1 and NEUROD1 Reveal Heterogeneity in Pulmonary Neuroendocrine Tumors and Regulate Distinct Genetic Programs. Cell reports 16, 1259–1272. [PubMed: 27452466]

Cao Y, He M, Gao Z, Peng Y, Li Y, Li L, Zhou W, Li X, Zhong X, Lei Y, et al. (2014). Activating hotspot L205R mutation in PRKACA and adrenal Cushing's syndrome. Science 344, 913–917. [PubMed: 24700472]

Chalkley RJ, Baker PR, Medzihradszky KF, Lynn AJ, and Burlingame AL (2008). In-depth analysis of tandem mass spectrometry data from disparate instrument types. Mol Cell Proteomics 7, 2386–2398. [PubMed: 18653769]

Chen EY, Tan CM, Kou Y, Duan Q, Wang Z, Meirelles GV, Clark NR, and Ma'ayan A (2013). Enrichr: interactive and collaborative HTML5 gene list enrichment analysis tool. BMC Bioinformatics 14, 128. [PubMed: 23586463]

Chen M, Gavrilova O, Zhao WQ, Nguyen A, Lorenzo J, Shen L, Nackers L, Pack S, Jou W, and Weinstein LS (2005). Increased glucose tolerance and reduced adiposity in the absence of fasting hypoglycemia in mice with liver-specific Gs alpha deficiency. J Clin Invest 115, 3217–3227. [PubMed: 16239968]

Choi M, Chang CY, Clough T, Broudy D, Killeen T, MacLean B, and Vitek O (2014). MSstats: an R package for statistical analysis of quantitative mass spectrometry-based proteomic experiments. Bioinformatics 30, 2524–2526. [PubMed: 24794931]

Cohen P (2002). Protein kinases--the major drug targets of the twenty-first century? Nat Rev Drug Discov 1, 309–315. [PubMed: 12120282]

Crooks GE, Hon G, Chandonia JM, and Brenner SE (2004). WebLogo: a sequence logo generator. Genome Res 14, 1188–1190. [PubMed: 15173120]

Cui M, Augert A, Rongione M, Conkrite K, Parazzoli S, Nikitin AY, Ingolia N, and Macpherson D (2014). PTEN is a Potent Suppressor of Small Cell Lung Cancer. Mol Cancer Res.

Deeble PD, Cox ME, Frierson HF Jr., Sikes RA, Palmer JB, Davidson RJ, Casarez EV, Amorino GP, and Parsons SJ (2007). Androgen-independent growth and tumorigenesis of prostate cancer cells are enhanced by the presence of PKA-differentiated neuroendocrine cells. Cancer Res 67, 3663–3672. [PubMed: 17440078]

Dobin A, Davis CA, Schlesinger F, Drenkow J, Zaleski C, Jha S, Batut P, Chaisson M, and Gingeras TR (2013). STAR: ultrafast universal RNA-seq aligner. Bioinformatics 29, 15–21. [PubMed: 23104886]

Dodge-Kafka KL, Bauman A, Mayer N, Henson E, Heredia L, Ahn J, McAvoy T, Nairn AC, and Kapiloff MS (2010). cAMP-stimulated protein phosphatase 2A activity associated with muscle A kinase-anchoring protein (mAKAP) signaling complexes inhibits the phosphorylation and activity of the cAMP-specific phosphodiesterase PDE4D3. J Biol Chem 285, 11078–11086. [PubMed: 20106966]

Doerr F, George J, Schmitt A, Beleggia F, Rehkamper T, Hermann S, Walter V, Weber JP, Thomas RK, Wittersheim M, et al. (2017). Targeting a non-oncogene addiction to the ATR/CHK1 axis for the treatment of small cell lung cancer. Scientific reports 7, 15511. [PubMed: 29138515]

Duncan JS, Whittle MC, Nakamura K, Abell AN, Midland AA, Zawistowski JS, Johnson NL, Granger DA, Jordan NV, Darr DB, et al. (2012). Dynamic reprogramming of the kinome in response to targeted MEK inhibition in triple-negative breast cancer. Cell 149, 307–321. [PubMed: 22500798]

Ferone G, Song JY, Krijsgsman O, van der Vliet J, Cozijnsen M, Semenova EA, Adams DJ, Peeper D, and Berns A (2020). FGFR oncogenic activation reveals an alternative cell-of-origin of SCLC in Rb1/p53 mice. Cell reports *in* press.

Gay CM, Tong P, Cardnell RJ, Sen T, Su X, Ma J, Bara RO, Johnson FM, Wakefield C, Heymach JV, et al. (2019). Differential Sensitivity Analysis for Resistant Malignancies (DISARM) Identifies Common Candidate Therapies across Platinum-Resistant Cancers. Clin Cancer Res 25, 346–357. [PubMed: 30257981]

Gazdar AF, Savage TK, Johnson JE, Berns A, Sage J, Linnoila RI, MacPherson D, McFadden DG, Farago A, Jacks T, et al. (2015). The comparative pathology of genetically engineered mouse models for neuroendocrine carcinomas of the lung. J Thorac Oncol 10, 553–564. [PubMed: 25675280]

George J, Lim JS, Jang SJ, Cun Y, Ozretic L, Kong G, Leenders F, Lu X, Fernandez-Cuesta L, Bosco G, et al. (2015). Comprehensive genomic profiles of small cell lung cancer. Nature 524, 47–53. [PubMed: 26168399]

Goh G, Scholl UI, Healy JM, Choi M, Prasad ML, Nelson-Williams C, Kunstman JW, Korah R, Suttorp AC, Dietrich D, et al. (2014). Recurrent activating mutation in PRKACA in cortisol-producing adrenal tumors. Nat Genet 46, 613–617. [PubMed: 24747643]

Gong X, Du J, Parsons SH, Merzoug FF, Webster Y, Iversen PW, Chio L-C, Van Horn RD, Lin X, and Blosser W (2019). Aurora A Kinase Inhibition Is Synthetic Lethal with Loss of the RB1 Tumor Suppressor Gene. Cancer discovery 9, 248–263. [PubMed: 30373917]

Grossman EA, Ward CC, Spradlin JN, Bateman LA, Huffman TR, Miyamoto DK, Kleinman JI, and Nomura DK (2017). Covalent Ligand Discovery against Druggable Hotspots Targeted by Anti-cancer Natural Products. Cell Chem Biol 24, 1368–1376 e1364. [PubMed: 28919038]

Hertz NT, Wang BT, Allen JJ, Zhang C, Dar AC, Burlingame AL, and Shokat KM (2010). Chemical genetic approach for kinase-substrate mapping by covalent capture of thiophosphopeptides and analysis by mass spectrometry. Current protocols in chemical biology 2, 15–36. [PubMed: 23836541]

Honeyman JN, Simon EP, Robine N, Chiaroni-Clarke R, Darcy DG, Lim II, Gleason CE, Murphy JM, Rosenberg BR, Teegan L, et al. (2014). Detection of a recurrent DNAJB1-PRKACA chimeric transcript in fibrolamellar hepatocellular carcinoma. Science 343, 1010–1014. [PubMed: 24578576]

Horn L, Mansfield AS, Szczesna A, Havel L, Krzakowski M, Hochmair MJ, Huemer F, Losonczy G, Johnson ML, Nishio M, et al. (2018). First-Line Atezolizumab plus Chemotherapy in Extensive-Stage Small-Cell Lung Cancer. N Engl J Med 379, 2220–2229. [PubMed: 30280641]

Horvath A, Bertherat J, Groussin L, Guillaud-Bataille M, Tsang K, Cazabat L, Libe R, Remmers E, Rene-Corail F, Faucz FR, et al. (2010). Mutations and polymorphisms in the gene encoding

regulatory subunit type 1-alpha of protein kinase A (PRKAR1A): an update. Hum Mutat 31, 369–379. [PubMed: 20358582]

Houslay MD, and Adams DR (2003). PDE4 cAMP phosphodiesterases: modular enzymes that orchestrate signalling cross-talk, desensitization and compartmentalization. Biochem J 370, 1–18. [PubMed: 12444918]

Hu Y, and Smyth GK (2009). ELDA: extreme limiting dilution analysis for comparing depleted and enriched populations in stem cell and other assays. J Immunol Methods 347, 70–78. [PubMed: 19567251]

Iglesias-Bartolome R, Torres D, Marone R, Feng X, Martin D, Simaan M, Chen M, Weinstein LS, Taylor SS, Molinolo AA, and Gutkind JS (2015). Inactivation of a Galpha(s)-PKA tumour suppressor pathway in skin stem cells initiates basal-cell carcinogenesis. Nat Cell Biol 17, 793–803. [PubMed: 25961504]

Imamura H, Sugiyama N, Wakabayashi M, and Ishihama Y (2014). Large-scale identification of phosphorylation sites for profiling protein kinase selectivity. J Proteome Res 13, 3410–3419. [PubMed: 24869485]

Isobe K, Jung HJ, Yang CR, Claxton J, Sandoval P, Burg MB, Raghuram V, and Knepper MA (2017). Systems-level identification of PKA-dependent signaling in epithelial cells. Proc Natl Acad Sci U S A 114, E8875–E8884. [PubMed: 28973931]

Jahchan NS, Dudley JT, Mazur PK, Flores N, Yang D, Palmerton A, Zmoos AF, Vaka D, Tran KQ, Zhou M, et al. (2013). A drug repositioning approach identifies tricyclic antidepressants as inhibitors of small cell lung cancer and other neuroendocrine tumors. Cancer Discov 3, 1364–1377. [PubMed: 24078773]

Jahchan NS, Lim JS, Bola B, Morris K, Seitz G, Tran KQ, Xu L, Trapani F, Morrow CJ, Cristea S, et al. (2016). Identification and Targeting of Long-Term Tumor-Propagating Cells in Small Cell Lung Cancer. Cell reports 16, 644–656. [PubMed: 27373157]

Jia D, Augert A, Kim DW, Eastwood E, Wu N, Ibrahim AH, Kim KB, Dunn CT, Pillai SPS, Gazdar AF, et al. (2018). Crebbp Loss Drives Small Cell Lung Cancer and Increases Sensitivity to HDAC Inhibition. Cancer Discov 8, 1422–1437. [PubMed: 30181244]

Kanie T, Abbott KL, Mooney NA, Plowey ED, Demeter J, and Jackson PK (2017). The CEP19-RABL2 GTPase Complex Binds IFT-B to Initiate Intraflagellar Transport at the Ciliary Base. Dev Cell 42, 22–36 e12. [PubMed: 28625565]

Kastenhuber ER, Lalazar G, Houlihan SL, Tschaharganeh DF, Baslan T, Chen CC, Requena D, Tian S, Bosbach B, Wilkinson JE, et al. (2017). DNAJB1-PRKACA fusion kinase interacts with beta-catenin and the liver regenerative response to drive fibrolamellar hepatocellular carcinoma. Proc Natl Acad Sci U S A 114, 13076–13084. [PubMed: 29162699]

Kastrinsky DB, Sangodkar J, Zaware N, Izadmehr S, Dhawan NS, Narla G, and Ohlmeyer M (2015). Reengineered tricyclic anti-cancer agents. Bioorg Med Chem 23, 6528–6534. [PubMed: 26372073]

Kirschner LS (2014). Medicine. A unified cause for adrenal Cushing's syndrome. Science 344, 804–805. [PubMed: 24855241]

Kirschner LS, Carney JA, Pack SD, Taymans SE, Giatzakis C, Cho YS, Cho-Chung YS, and Stratakis CA (2000). Mutations of the gene encoding the protein kinase A type I-alpha regulatory subunit in patients with the Carney complex. Nat Genet 26, 89–92. [PubMed: 10973256]

Lallo A, Frese KK, Morrow CJ, Sloane R, Gulati S, Schenk MW, Trapani F, Simms N, Galvin M, Brown S, et al. (2018). The Combination of the PARP Inhibitor Olaparib and the WEE1 Inhibitor AZD1775 as a New Therapeutic Option for Small Cell Lung Cancer. Clin Cancer Res 24, 5153–5164. [PubMed: 29941481]

Landis CA, Masters SB, Spada A, Pace AM, Bourne HR, and Vallar L (1989). GTPase inhibiting mutations activate the alpha chain of Gs and stimulate adenylyl cyclase in human pituitary tumours. Nature 340, 692–696. [PubMed: 2549426]

Leong TL, Marini KD, Rossello FJ, Jayasekara SN, Russell PA, Prodanovic Z, Kumar B, Ganju V, Alamgeer M, Irving LB, et al. (2014). Genomic characterisation of small cell lung cancer patient-derived xenografts generated from endobronchial ultrasound-guided transbronchial needle aspiration specimens. PLoS One 9, e106862. [PubMed: 25191746]

Levin RS, Hertz NT, Burlingame AL, Shokat KM, and Mukherjee S (2016). Innate immunity kinase TAK1 phosphorylates Rab1 on a hotspot for posttranslational modifications by host and pathogen. Proc Natl Acad Sci U S A 113, E4776–4783. [PubMed: 27482120]

Li B, Ding S, Feng N, Mooney N, Ooi YS, Ren L, Diep J, Kelly MR, Yasukawa LL, Patton JT, et al. (2017). Drebrin restricts rotavirus entry by inhibiting dynamin-mediated endocytosis. Proc Natl Acad Sci U S A 114, E3642–E3651. [PubMed: 28416666]

Li L, Ng SR, Colon CI, Drapkin BJ, Hsu PP, Li Z, Nabel CS, Lewis CA, Romero R, Mercer KL, et al. (2019). Identification of DHODH as a therapeutic target in small cell lung cancer. Sci Transl Med 11.

Lim JS, Ibaseta A, Fischer MM, Cancilla B, O'Young G, Cristea S, Luca VC, Yang D, Jahchan NS, Hamard C, et al. (2017). Intratumoural heterogeneity generated by Notch signalling promotes small-cell lung cancer. Nature 545, 360–364. [PubMed: 28489825]

Lipp JJ, Marvin MC, Shokat KM, and Guthrie C (2015). SR protein kinases promote splicing of nonconsensus introns. Nat Struct Mol Biol 22, 611–617. [PubMed: 26167880]

Logue JS, and Scott JD (2010). Organizing signal transduction through A-kinase anchoring proteins (AKAPs). FEBS J 277, 4370–4375. [PubMed: 20883492]

Love MI, Huber W, and Anders S (2014). Moderated estimation of fold change and dispersion for RNA-seq data with DESeq2. Genome Biol 15, 550. [PubMed: 25516281]

Manchado E, Weissmueller S, Morris J. P. t., Chen CC, Wullenkord R, Lujambio A, de Stanchina E, Poirier JT, Gainor JF, Corcoran RB, et al. (2016). A combinatorial strategy for treating KRAS-mutant lung cancer. Nature 534, 647–651. [PubMed: 27338794]

Manning G, Whyte DB, Martinez R, Hunter T, and Sudarsanam S (2002). The protein kinase complement of the human genome. Science 298, 1912–1934. [PubMed: 12471243]

Marcotte R, Sayad A, Brown KR, Sanchez-Garcia F, Reimand J, Haider M, Virtanen C, Bradner JE, Bader GD, Mills GB, et al. (2016). Functional Genomic Landscape of Human Breast Cancer Drivers, Vulnerabilities, and Resistance. Cell 164, 293–309. [PubMed: 26771497]

Mazhar S, Taylor SE, Sangodkar J, and Narla G (2019). Targeting PP2A in cancer: Combination therapies. Biochim Biophys Acta Mol Cell Res 1866, 51–63. [PubMed: 30401535]

McFadden DG, Papagiannakopoulos T, Taylor-Weiner A, Stewart C, Carter SL, Cibulskis K, Bhutkar A, McKenna A, Dooley A, Vernon A, et al. (2014). Genetic and clonal dissection of murine small cell lung carcinoma progression by genome sequencing. Cell 156, 1298–1311. [PubMed: 24630729]

McFarland JM, Ho ZV, Kugener G, Dempster JM, Montgomery PG, Bryan JG, Krill-Burger JM, Green TM, Vazquez F, Boehm JS, et al. (2018). Improved estimation of cancer dependencies from large-scale RNAi screens using model-based normalization and data integration. Nat Commun 9, 4610. [PubMed: 30389920]

Mollaoglu G, Guthrie MR, Bohm S, Bragelmann J, Can I, Ballieu PM, Marx A, George J, Heinen C, Chalishazar MD, et al. (2017). MYC Drives Progression of Small Cell Lung Cancer to a Variant Neuroendocrine Subtype with Vulnerability to Aurora Kinase Inhibition. Cancer Cell 31, 270–285. [PubMed: 28089889]

Moore CE, Xie J, Gomez E, and Herbert TP (2009). Identification of cAMP-dependent kinase as a third in vivo ribosomal protein S6 kinase in pancreatic beta-cells. J Mol Biol 389, 480–494. [PubMed: 19376132]

Morgan DJ, Weisenhaus M, Shum S, Su T, Zheng R, Zhang C, Shokat KM, Hille B, Babcock DF, and McKnight GS (2008). Tissue-specific PKA inhibition using a chemical genetic approach and its application to studies on sperm capacitation. Proc Natl Acad Sci U S A 105, 20740–20745. [PubMed: 19074277]

Mukhopadhyay S, Wen X, Ratti N, Loktev A, Rangell L, Scales SJ, and Jackson PK (2013). The ciliary G-protein-coupled receptor Gpr161 negatively regulates the Sonic hedgehog pathway via cAMP signaling. Cell 152, 210–223. [PubMed: 23332756]

Musante V, Li L, Kanyo J, Lam TT, Colangelo CM, Cheng SK, Brody AH, Greengard P, Le Novere N, and Nairn AC (2017). Reciprocal regulation of ARPP-16 by PKA and MAST3 kinases provides a cAMP-regulated switch in protein phosphatase 2A inhibition. eLife 6.

Nagai T, Nakamuta S, Kuroda K, Nakauchi S, Nishioka T, Takano T, Zhang X, Tsuboi, , Funahashi Y, Nakano T, et al. (2016). Phosphoproteomics of the Dopamine Pathway Enables Discovery of Rap1 Activation as a Reward Signal In Vivo. Neuron 89, 550–565. [PubMed: 26804993]

Novak D, Huser L, Elton JJ, Umansky V, Altevogt P, and Utikal J (2019). SOX2 in development and cancer biology. Semin Cancer Biol.

Orellana SA, and McKnight GS (1992). Mutations in the catalytic subunit of cAMP-dependent protein kinase result in unregulated biological activity. Proc Natl Acad Sci U S A 89, 4726–4730. [PubMed: 1584809]

Oser MG, Fonseca R, Chakraborty AA, Brough R, Spektor A, Jennings RB, Flaifel A, Novak JS, Gulati A, and Buss E (2019). Cells lacking the RB1 tumor suppressor gene are hyperdependent on Aurora B kinase for survival. Cancer discovery 9, 230–247. [PubMed: 30373918]

Park KS, Martelotto LG, Peifer M, Sos ML, Karnezis AN, Mahjoub MR, Bernard K, Conklin JF, Szczepny A, Yuan J, et al. (2011). A crucial requirement for Hedgehog signaling in small cell lung cancer. Nat Med 17, 1504–1508. [PubMed: 21983857]

Pattabiraman DR, Bierie B, Kober KI, Thiru P, Krall JA, Zill C, Reinhardt F, Tam W, and Weinberg RA (2016). Activation of PKA leads to mesenchymal-to-epithelial transition and loss of tumor-initiating ability. Science 351, aad3680. [PubMed: 26941323]

Peifer M, Fernandez-Cuesta L, Sos ML, George J, Seidel D, Kasper LH, Plenker D, Leenders F, Sun R, Zander T, et al. (2012). Integrative genome analyses identify key somatic driver mutations of small-cell lung cancer. Nat Genet 44, 1104–1110. [PubMed: 22941188]

Pietanza MC, Byers LA, Minna JD, and Rudin CM (2015). Small cell lung cancer: will recent progress lead to improved outcomes? Clin Cancer Res 21, 2244–2255. [PubMed: 25979931]

Poirier JT, Gardner EE, Connis N, Moreira AL, de Stanchina E, Hann CL, and Rudin CM (2015). DNA methylation in small cell lung cancer defines distinct disease subtypes and correlates with high expression of EZH2. Oncogene 34, 5869–5878. [PubMed: 25746006]

Ready NE, Ott PA, Hellmann MD, Zugazagoitia J, Hann CL, de Braud F, Antonia SJ, Ascierto PA, Moreno V, Atmaca A, et al. (2019). Nivolumab Monotherapy and Nivolumab Plus Ipilimumab in Recurrent Small Cell Lung Cancer: Results From the CheckMate 032 Randomized Cohort. J Thorac Oncol.

Roskoski R Jr. (2016). Classification of small molecule protein kinase inhibitors based upon the structures of their drug-enzyme complexes. Pharmacol Res 103, 26–48. [PubMed: 26529477]

Rudin CM, Durinck S, Stawiski EW, Poirier JT, Modrusan Z, Shames DS, Bergbower EA, Guan Y, Shin J, Guillory J, et al. (2012). Comprehensive genomic analysis identifies SOX2 as a frequently amplified gene in small-cell lung cancer. Nat Genet 44, 1111–1116. [PubMed: 22941189]

Rudin CM, Poirier JT, Byers LA, Dive C, Dowlati A, George J, Heymach JV, Johnson JE, Lehman JM, MacPherson D, et al. (2019). Molecular subtypes of small cell lung cancer: a synthesis of human and mouse model data. Nat Rev Cancer.

Sabari JK, Lok BH, Laird JH, Poirier JT, and Rudin CM (2017). Unravelling the biology of SCLC: implications for therapy. Nature reviews Clinical oncology 14, 549–561.

Saloustros E, Salpea P, Starost M, Liu S, Faucz FR, London E, Szarek E, Song WJ, Hussain M, and Stratakis CA (2017). Prkar1a gene knockout in the pancreas leads to neuroendocrine tumorigenesis. Endocr Relat Cancer 24, 31–40. [PubMed: 27803029]

Salpea P, and Stratakis CA (2014). Carney complex and McCune Albright syndrome: an overview of clinical manifestations and human molecular genetics. Mol Cell Endocrinol 386, 85–91. [PubMed: 24012779]

Sangodkar J, Perl A, Tohme R, Kiselar J, Kastrinsky DB, Zaware N, Izadmehr S, Mazhar S, Wiredja DD, O'Connor CM, et al. (2017). Activation of tumor suppressor protein PP2A inhibits KRAS-driven tumor growth. J Clin Invest 127, 2081–2090. [PubMed: 28504649]

Sato Y, Maekawa S, Ishii R, Sanada M, Morikawa T, Shiraishi Y, Yoshida K, Nagata Y, Sato-Otsubo A, Yoshizato T, et al. (2014). Recurrent somatic mutations underlie corticotropin-independent Cushing's syndrome. Science 344, 917–920. [PubMed: 24855271]

Saunders LR, Bankovich AJ, Anderson WC, Aujay MA, Bheddah S, Black K, Desai R, Escarpe PA, Hampl J, Laysang A, et al. (2015). A DLL3-targeted antibody-drug conjugate eradicates high-grade pulmonary neuroendocrine tumor-initiating cells in vivo. Sci Transl Med 7, 302ra136.

Schaffer BE, Park KS, Yiu G, Conklin JF, Lin C, Burkhart DL, Karnezis AN, Sweet-Cordero EA, and Sage J (2010). Loss of p130 accelerates tumor development in a mouse model for human small-cell lung carcinoma. Cancer Res 70, 3877–3883. [PubMed: 20406986]

Schauble S, King CC, Darshi M, Koller A, Shah K, and Taylor SS (2007). Identification of ChChd3 as a novel substrate of the cAMP-dependent protein kinase (PKA) using an analog-sensitive catalytic subunit. J Biol Chem 282, 14952–14959. [PubMed: 17242405]

Schilling B, Rardin MJ, MacLean BX, Zawadzka AM, Frewen BE, Cusack MP, Sorensen DJ, Bereman MS, Jing E, Wu CC, et al. (2012). Platform-independent and label-free quantitation of proteomic data using MS1 extracted ion chromatograms in skyline: application to protein acetylation and phosphorylation. Mol Cell Proteomics 11, 202–214. [PubMed: 22454539]

Sen T, Tong P, Diao L, Li L, Fan Y, Hoff J, Heymach JV, Wang J, and Byers LA (2017a). Targeting AXL and mTOR Pathway Overcomes Primary and Acquired Resistance to WEE1 Inhibition in Small-Cell Lung Cancer. Clin Cancer Res 23, 6239–6253. [PubMed: 28698200]

Sen T, Tong P, Stewart CA, Cristea S, Valliani A, Shames DS, Redwood AB, Fan YH, Li L, Glisson BS, et al. (2017b). CHK1 Inhibition in Small-Cell Lung Cancer Produces Single-Agent Activity in Biomarker-Defined Disease Subsets and Combination Activity with Cisplatin or Olaparib. Cancer Res 77, 3870–3884. [PubMed: 28490518]

Shannon P, Markiel A, Ozier O, Baliga NS, Wang JT, Ramage D, Amin N, Schwikowski B, and Ideker T (2003). Cytoscape: a software environment for integrated models of biomolecular interaction networks. Genome Res 13, 2498–2504. [PubMed: 14597658]

Skalhegg BS, Huang Y, Su T, Idzerda RL, McKnight GS, and Burton KA (2002). Mutation of the Calpha subunit of PKA leads to growth retardation and sperm dysfunction. Mol Endocrinol 16, 630–639. [PubMed: 11875122]

Sos ML, Dietlein F, Peifer M, Schottle J, Balke-Want H, Muller C, Koker M, Richters A, Heynck S, Malchers F, et al. (2012). A framework for identification of actionable cancer genome dependencies in small cell lung cancer. Proc Natl Acad Sci U S A 109, 17034–17039. [PubMed: 23035247]

Sos ML, Levin RS, Gordan JD, Oses-Prieto JA, Webber JT, Salt M, Hann B, Burlingame AL, McCormick F, Bandyopadhyay S, and Shokat KM (2014). Oncogene Mimicry as a Mechanism of Primary Resistance to BRAF Inhibitors. Cell reports 8, 1037–1048. [PubMed: 25127139]

Spandidos A, Wang X, Wang H, and Seed B (2010). PrimerBank: a resource of human and mouse PCR primer pairs for gene expression detection and quantification. Nucleic Acids Res 38, D792–799. [PubMed: 19906719]

Swaney DL, and Villen J (2016). Enrichment of Phosphopeptides via Immobilized Metal Affinity Chromatography. Cold Spring Harb Protoc 2016, pdb prot088005.

Teicher BA (2014). Targets in small cell lung cancer. Biochem Pharmacol 87, 211–219. [PubMed: 24091017]

Torres JZ, Miller JJ, and Jackson PK (2009). High-throughput generation of tagged stable cell lines for proteomic analysis. Proteomics 9, 2888–2891. [PubMed: 19405035]

Uys GM, Ramburan A, Loos B, Kinnear CJ, Korkie LJ, Mouton J, Riedemann J, and Moolman-Smook JC (2011). Myomegalin is a novel A-kinase anchoring protein involved in the phosphorylation of cardiac myosin binding protein C. BMC Cell Biol 12, 18. [PubMed: 21569246]

Vintonyak VV, Antonchick AP, Rauh D, and Waldmann H (2009). The therapeutic potential of phosphatase inhibitors. Curr Opin Chem Biol 13, 272–283. [PubMed: 19410499]

Vizcaino JA, Csordas A, Del-Toro N, Dianes JA, Griss J, Lavidas I, Mayer G, Perez-Riverol Y, Reisinger F, Ternent T, et al. (2016). 2016 update of the PRIDE database and its related tools. Nucleic Acids Res 44, 11033. [PubMed: 27683222]

Weinstein LS, Shenker A, Gejman PV, Merino MJ, Friedman E, and Spiegel AM (1991). Activating mutations of the stimulatory G protein in the McCune-Albright syndrome. N Engl J Med 325, 1688–1695. [PubMed: 1944469]

Wu N, Jia D, Ibrahim AH, Bachurski CJ, Gronostajski RM, and MacPherson D (2016). NFIB overexpression cooperates with Rb/p53 deletion to promote small cell lung cancer. Oncotarget 7, 57514–57524. [PubMed: 27613844]

Xia Y, Zhan C, Feng M, Leblanc M, Ke E, Yeddula N, and Verma IM (2018). Targeting CREB Pathway Suppresses Small Cell Lung Cancer. Mol Cancer Res 16, 825–832. [PubMed: 29523765]

Xu L, Hazard FK, Zmoos AF, Jahchan N, Chaib H, Garfin PM, Rangaswami A, Snyder MP, and Sage J (2015). Genomic analysis of fibrolamellar hepatocellular carcinoma. Hum Mol Genet 24, 50–63. [PubMed: 25122662]

Zakany R, Szucs K, Bako E, Felszeghy S, Czifra G, Biro T, Modis L, and Gergely P (2002). Protein phosphatase 2A is involved in the regulation of protein kinase A signaling pathway during in vitro chondrogenesis. Exp Cell Res 275, 1–8. [PubMed: 11925100]

Zhang J, Yang PL, and Gray NS (2009). Targeting cancer with small molecule kinase inhibitors. Nat Rev Cancer 9, 28–39. [PubMed: 19104514]

Zheng Y, de la Cruz CC, Sayles LC, Alleyne-Chin C, Vaka D, Knaak TD, Bigos M, Xu Y, Hoang CD, Shrager JB, et al. (2013). A Rare Population of CD24(+)ITGB4(+)Notch(hi) Cells Drives Tumor Propagation in NSCLC and Requires Notch3 for Self-Renewal. Cancer Cell 24, 59–74. [PubMed: 23845442]

Zhou Y, Zhou B, Pache L, Chang M, Khodabakhshi AH, Tanaseichuk O, Benner C, and Chanda SK (2019). Metascape provides a biologist-oriented resource for the analysis of systems-level datasets. Nature communications 10, 1523.

SIGNIFICANCE

Rare human genetic syndromes in which mutations activate PKA signaling are associated with the development of a spectrum of neuroendocrine tumors. Here, we show that the PKA signaling pathway is also active and critical for the growth of SCLC, a frequent and fatal form of neuroendocrine cancer. Furthermore, through a comprehensive proteomic analysis of SCLC tumors and cell lines, we identified proteins in the PKA holoenzyme network as well as a large number of potential targets of PKA. These data provide one of the largest and most diverse proteomic datasets exploring PKA signaling, and this resource should yield insight into the mechanisms driving SCLC progression as well as other PKA-dependent and G protein-coupled receptor (GPCR)-activated neuroendocrine cancers.

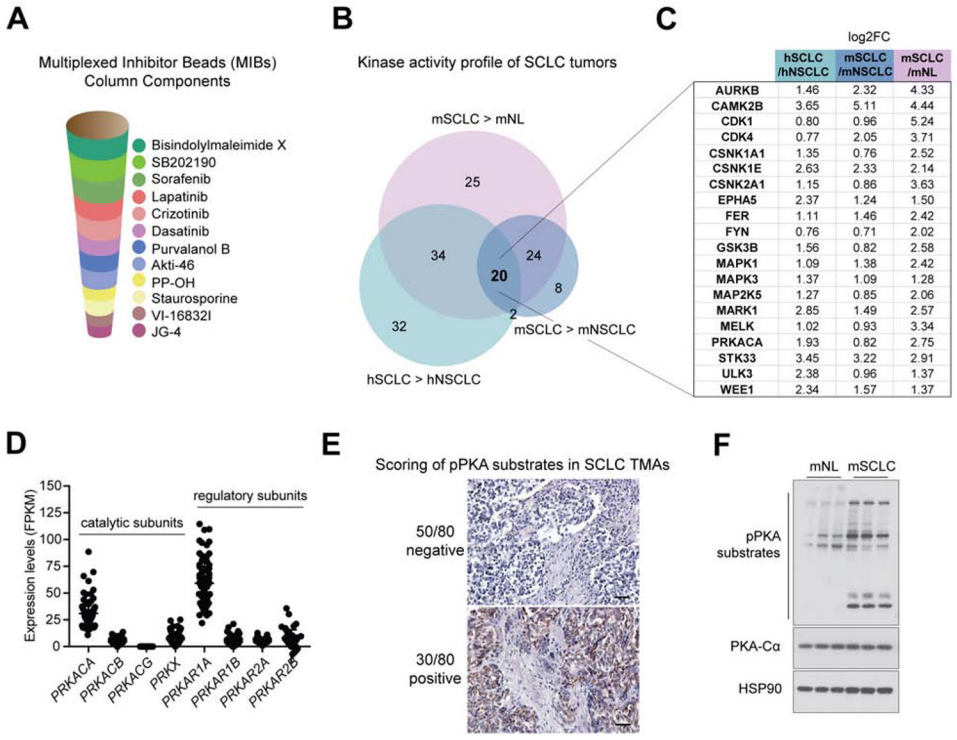

Figure 1: MIBs kinome profiling identifies PKA and other active kinases in SCLC

(A) Multiplexed Inhibitor Beads (MIBs) columns to enrich for active kinases in SCLC, using non-SCLC (NSCLC) and mouse normal lungs (mNL) as controls. Layers with inhibitors are shown. (B) Venn diagram of the candidate active kinases identified from the MIBs assay after mass spectrometry analysis using lysates from mouse (m) and human (h) SCLC and NSCLC tumors and mNL. (C) List of the 20 kinases (alphabetical order, gene names) found to be significantly more active in SCLC over controls, along with the log2-fold change (log2FC) of their enrichment. (D) RNA-seq expression levels of PKA catalytic and regulatory subunit genes in 81 human SCLC tumors. (E) PKA activity scored by immunohistochemistry of phosphorylated PKA (pPKA) substrates on human SCLC tissue microarrays (TMAs). Negative staining was based on no signal (n=22) or blush/weak signal (n=28). Positive staining was based on moderate staining (n=24) or strong staining (n=6). Scale bar is 100 μm. (F) Immunoblot for PKA-Cα and pPKA substrates in mNL and mouse SCLC (mSCLC). HSP90 is as a loading control.

See also Figure S1, and Table S1.

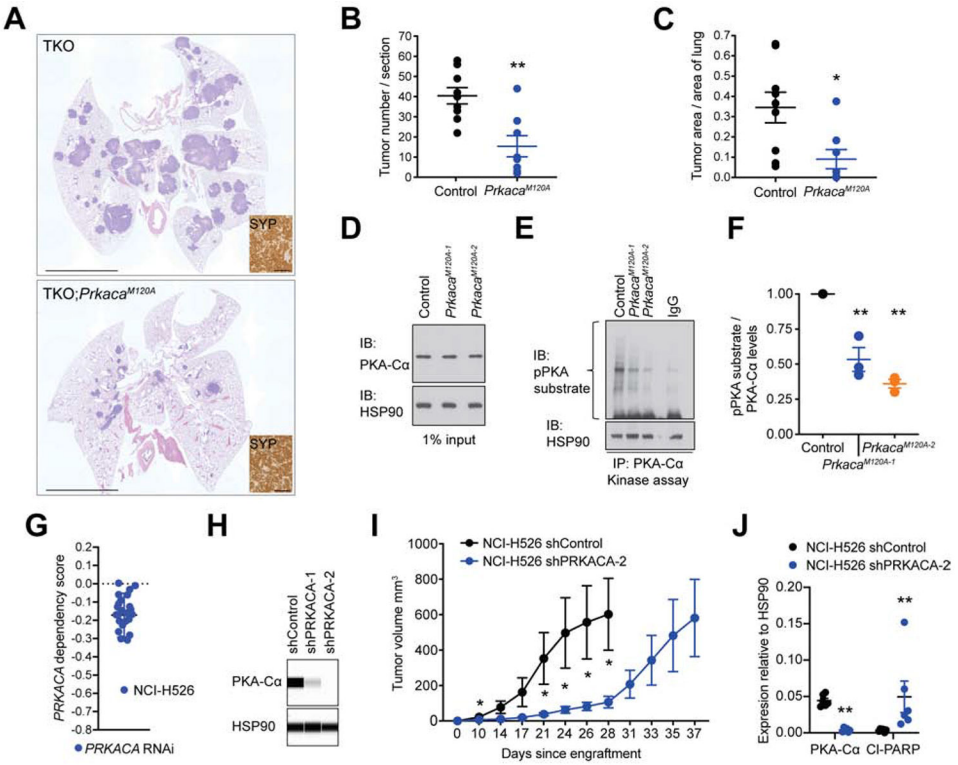

Figure 2: PKA is required for the growth of SCLC

(A) Representative images of sections counterstained with hematoxylin and eosin (H&E) from the lungs of TKO (control) and TKO;*Prkaca*$^{M120A/M120A}$ (*Prkaca*^{M120A}) mice 5 months after Ad-Cre. Scale bar, 5 mm. Insets show representative Synaptophysin (SYP) immunostaining (brown signal). Scale bar, 100 μm. (B-C) Quantification of tumor numbers (B) and tumor area (C) (n=8-9 mice/group). ** p=0.0016 and *p=0.0142. (D) Immunoblot (IB) for PKA-Cα levels in TKO (control) and TKO;*Prkaca*^{M120A} SCLC cell cultures (from independent tumors). HSP90 is a loading control. (E) Immunoblot for phospho-PKA substrates (pPKA) following *in vitro* kinase reactions using immunoprecipitated (IP) PKA-Cα from TKO (control) or TKO;*Prkaca*^{M120A} SCLC cell cultures. A native tumor extract was used as the kinase substrate. HSP90 is a loading control. A substrate-only lane with IgG control kinase reaction is shown. (F) Quantification of PKA kinase activity in a control TKO and two TKO;*Prkaca*^{M120A} SCLC cell cultures (n=3). M120A-1 p=0.0054**, M120A-2 p<0.0001**. (G) DepMap analysis of the requirement for PRKACA in human SCLC cells. (H) Immunoassay for PKA-Cα levels in control (shControl) and PRKACA knockdown (shPRKACA) human NCI-H526 SCLC cells. HSP90 is a loading control. (I) Growth of shControl and shPRKACA NCI-H526 xenografts in NSG mice (n=12 tumors/group). Day 10 p=0.036*, 21 p=0.041*, 24 p=0.040*, 26 p=0.032*, 28 p=0.024*. (J) Quantification of expression of PKA-Cα and cleaved PARP (Cl-PARP) by immunoassay (n=6 tumors closest to the mean) (see Figure S2K). PKA-Cα p=0.002**, Cl-PARP p=0.002**.

Data are presented as mean ± SEM. See also Figure S2.

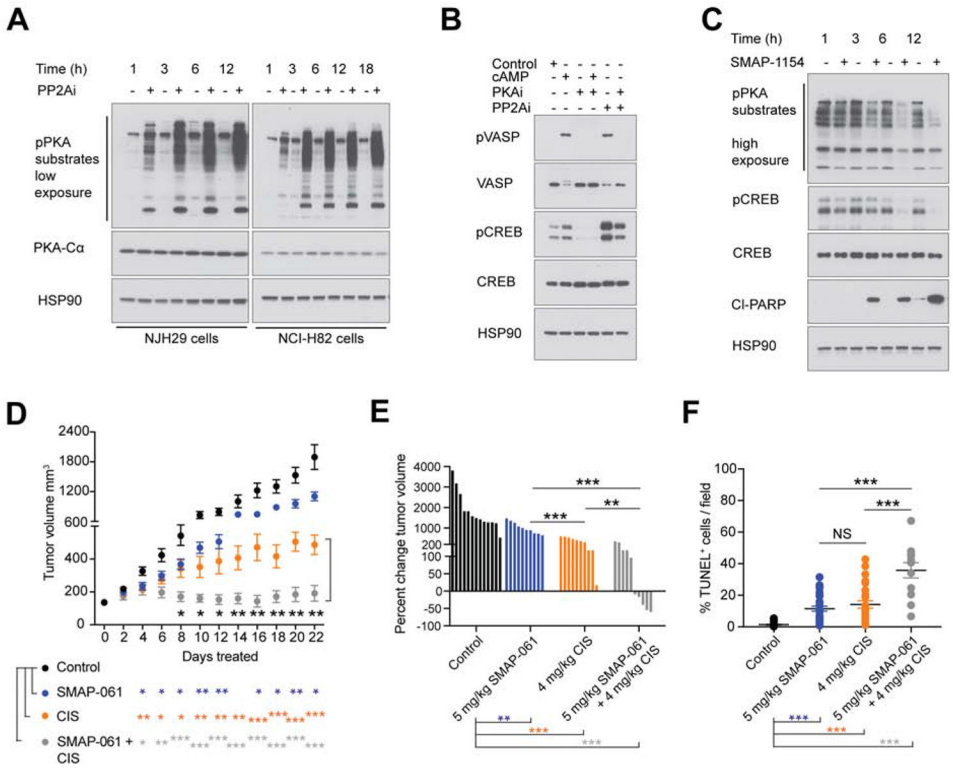

Figure 3: PP2A de-phosphorylates PKA substrates and inhibits the growth of SCLC

(A) Immunoblot for phosphorylated PKA substrates (pPKA) and PKA-Cα from NJH29 and NCI-H82 cells treated with 10 μM PP2Ai for increasing amounts of time. HSP90 is a loading control. (B) Immunoblot for the indicated proteins from NJH29 cells treated with 100 μM 8-Br-cAMP, 20 μM H89 (PKAi), and/or 10 μM PP2Ai. (C) Immunoblot for the indicated proteins from NJH29 cells treated with 10 μM of SMAP-1154 for various amounts of time. HSP90 is a loading control. (D-E) Growth curve (D) and waterfall plot (E) of NCI-H69 xenografts treated with SMAP DT-061 (labeled SMAP-061), Cisplatin, or SMAP-061 and Cisplatin (n=10-13). (F) Quantification of TUNEL staining of NCI-H69 SCLC tumors from (D).

Data are presented as mean ± SEM. NS, not significant, $p<0.05$*, $p<0.01$**, $p<0.001$.

See also Figure S3.

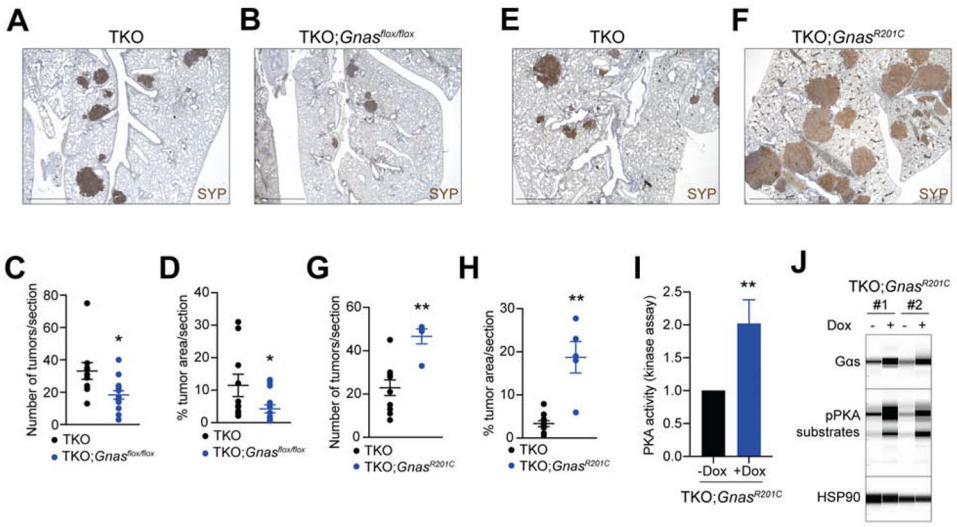

Figure 4: Gαs is necessary and sufficient for the growth of SCLC

(A-B) Representative images of sections immunostained for Synaptophysin (SYP) and counterstained with hematoxylin from the lungs of TKO (A) and TKO;*Gnas*$^{flox/flox}$ (B) mice 5 months after cancer initiation. Scale bar, 5 mm. (C-D) Quantification of tumor numbers (C, p=0.027*) and tumor area (D, p=0.022*) from (A-B) (n=10-14 mice/group). (E-F) Representative images of sections immunostained for SYP and counterstained with hematoxylin from the lungs of TKO and TKO;*Gnas*^{R201C} mice 5 months after cancer initiation, including the last 6 weeks with doxycycline (Dox) treatment to induce Gαs^{R201C}. Scale bar, 5 mm. (G-H) Quantification of tumor numbers (G, p=0.0011**) and tumor area (H, p=0.0013**) for SYP-positive lesions (n=5-10 mice/group) from (E-F). (I-J) Kinase activity assay for PKA (I) (n=6, p=0.0022**) and immunoassay for phospho-PKA (pPKA) substrates and Gαs protein levels (J) in two independent primary cultures from TKO;*Gnas*^{R201C} cells with or without Dox. HSP90 is a loading control.
Data are presented as mean ± SEM. See also Figure S4.

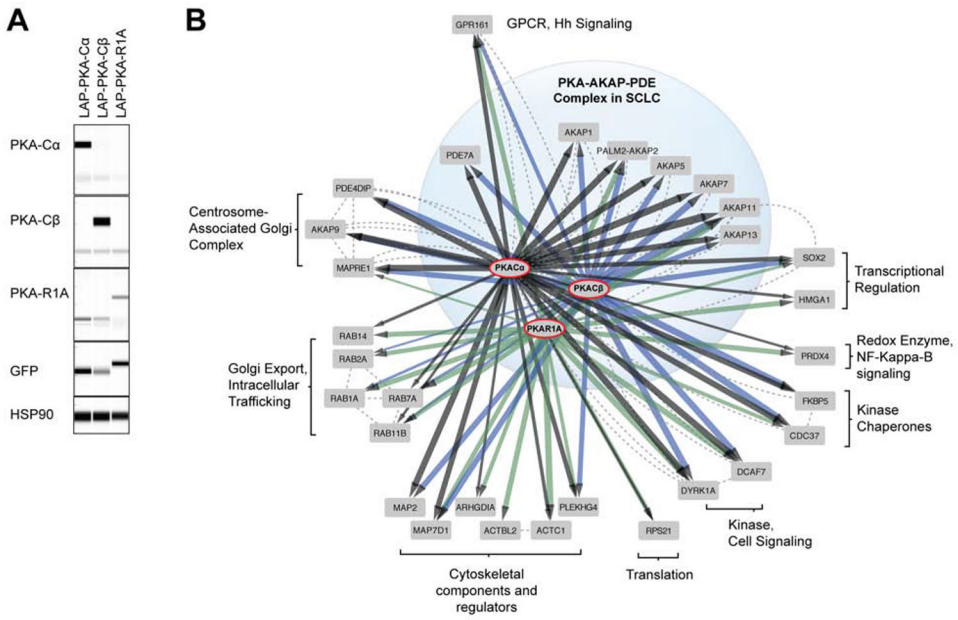

Figure 5: The PKA interactome in SCLC cells

(A) Expression of PKA-Cα, PKA-Cβ, and PKA-R1A in human NCI-H446 SCLC cells expressing stable LAP-tagged versions of these proteins measured by immunoassay. GFP is part of the LAP tag. HSP90 is a loading control. (B) Cytoscape network depicting a high confidence protein-protein interaction network for proteins pulled down by PKA-Cα, PKA-Cβ, and PKA-R1A. Only proteins pulled down by more than one bait are shown. Proteins in the light blue circle are part of the core PKA interactome including PKA catalytic and regulatory subunits, A-kinase anchoring proteins (AKAPs), and phosphodiesterases (PDEs). The thickness of the lines denotes the strength of interaction (padj<0.05) and the color represents interaction with the bait. Dashed lines show known interactions from BioGRID. See also Figure S5 and Table S2.

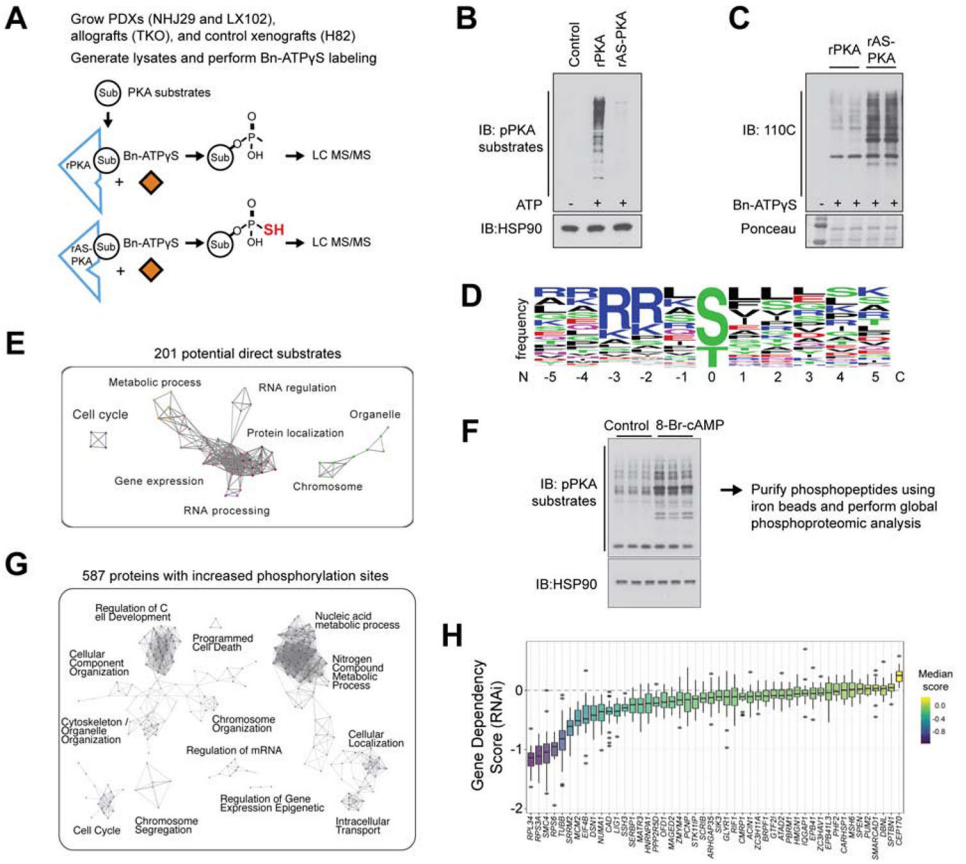

Figure 6: PKA controls a large and diverse set of downstream processes in SCLC cells

(A) Analog-specific (AS) approach used to identify direct PKA-Cα substrates in SCLC. (B) *In vitro* kinase assays followed by immunoblot with NJH29 tumor extracts using recombinant PKA (rPKA) or recombinant analog-sensitive PKA (rAS-PKA). The pPKA antibody identifies phosphorylated PKA substrates. HSP90 is a loading control. (C) *In vitro* kinase assays performed as in (B) except that the bulky Bn-ATPγS analog was used as an ATP donor and the 110C antibody was used to detect thiophosphorylated proteins. (D) Motif analysis for the candidate direct PKA-Cα substrates identified with the rAS-PKA enzyme. (E) Nodes of GO terms of the biological processes in which the candidate PKA substrates are implicated. (F) Overview of the global phosphoproteomic approach to identify signaling events downstream of PKA activation by 8-Br-cAMP. Data with NCI-H69 cells are shown. The pPKA substrates immunoblot is a positive control. HSP90 is a loading control. (G) Nodes of GO terms of biological processes altered by activation of PKA after analysis of the global phosphoproteomic data (cases with increased phosphorylation). (H) Box-and-whiskers plot of the DepMap (RNAi) gene dependency score for candidate PKA substrates (n=48). Lower and upper parts of the box correspond to the 25th and 75th percentiles, respectively, and the whiskers extend to 1.5x interquartile range (IQR). Median value is noted by the thick line within the box, and individual dots represent scores that lie outside 1.5x IQR.

See also Figure S6, and Tables S3-S5.

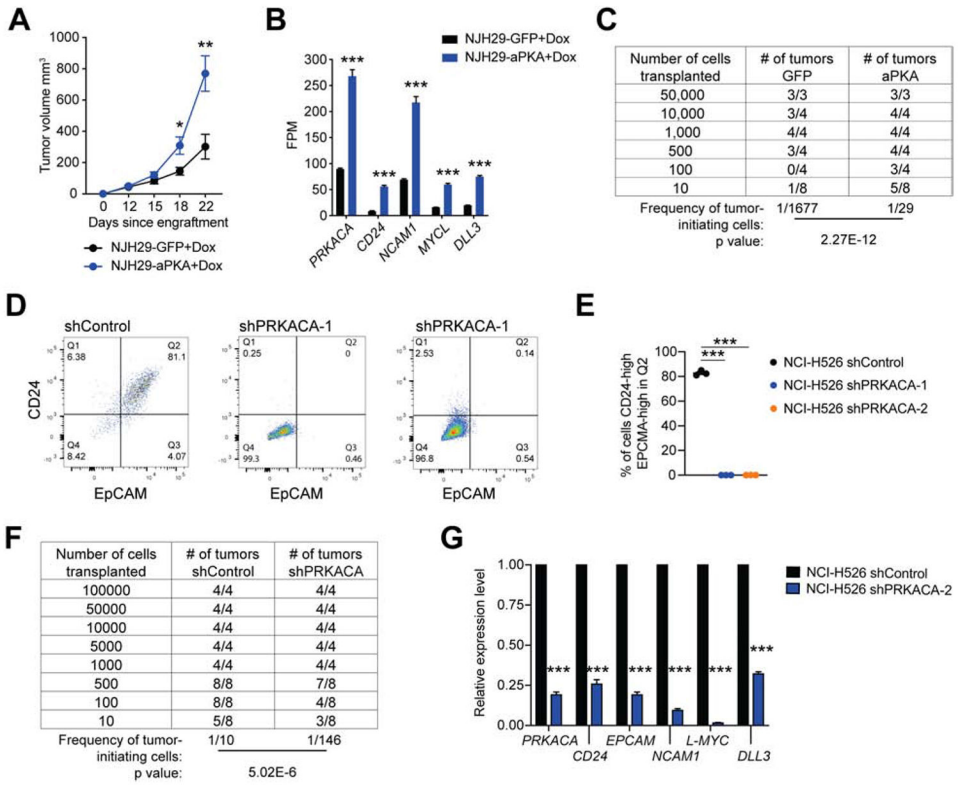

Figure 7: PKA activity promotes the expansion of SCLC cancer stem Cells

(A) Growth of NJH29 xenografts expressing GFP or an active form of PKA-Cα (aPKA). n=9, Day 18 p=0.015*, Day 22 p=0.003**; data are presented as mean ± SEM. Dox=Doxycycline (B) Levels of *PRKACA* and marker genes associated with SCLC cancer stem cells in NJH29 xenografts from RNA-seq data. n=4, *PRKACA* padj<0.0001***, *CD24* padj<0.0001***, *NCAM1* padj<0.0001***, *L-MYC* padj<0.0001***, *DLL3* padj<0.0001***; data are presented as mean ± SEM. (C) Transplantation studies with various numbers of NHJ29 cells expressing GFP or aPKA (n=3-8 tumors per dilution). The calculated frequency of tumor-initiating cells is indicated along with the p value. (D) Expression of CD24 and EPCAM in NCI-H526 cells in control and *PRKACA* knockdown cells measured by flow cytometry. (E) Quantification of $CD24^{High}$ $EPCAM^{High}$ cells (quadrant 2 (Q2)) from D. (n=3, p<0.0001). (F) Transplantation studies with various numbers of control and *PRKACA* knockdown NCI-H526 cells (n=4-8 tumors per dilution). The calculated frequency of tumor-initiating cells is indicated along with the p value. (G) Expression of *PRKACA* and genes associated with SCLC cancer stem cells in control and *PRKACA* knockdown NCI-H526 xenografts measured by RT-qPCR. n=5, p<0.0001*** for all genes tested. data are presented as mean ± SEM.

See also Figure S7 and Table S6.

KEY RESOURCES TABLE

REAGENT or RESOURCE	SOURCE	IDENTIFIER
Antibodies		
pPKA substrates	Cell Signaling Technology	Cat#9621, Cat#9624
PRKACA	Cell Signaling Technology	Cat#4782
PRKACB	Santa Cruz	Cat#904
PRKAR1A/B	Cell Signaling Technology	Cat#39275
HSP90	Cell Signaling Technology	Cat#4877
Cleaved PARP	Cell Signaling Technology	Cat#5625, Cat#9548
TUBULIN	Developmental Studies Hybridoma Bank	Cat#E7
Cleaved CASPASE 3	Cell Signaling Technology	Cat#9509
p-Histone H3	Cell Signaling Technology	Cat#53348
PCNA	Santa Cruz	Cat#sc-56
pCREB^{S133}	Cell Signaling Technology	Cat#9198
CREB	Cell Signaling Technology	Cat#9197
pVASP^{S157}	Cell Signaling Technology	Cat#84519
Ki67	Thermo Fisher	Cat#RM-9106
VASP	Cell Signaling Technology	Cat#3132
p-MYC-C^{S62}	Cell Signaling Technology	Cat#13748
MYC-C	Cell Signaling Technology	Cat#5605
pMTOR^{S2448}	Cell Signaling Technology	Cat#2971
MTOR	Cell Signaling Technology	Cat#2972
ASCL1	BD Biosciences	Cat#556604
NEUROD1	Cell Signaling Technology	Cat#4373
NFIB	Abcam	Cat#ab186738
HES1	Cell Signaling Technology	Cat#11988
NCAM1	Millipore	Cat#AB5032
DLL3	Sigma-Aldrich	Cat#HPA056533
INSM1	Santa Cruz	Cat#sc-271408
GFP	Invitrogen	Cat#A11122
SYP	Neuromics	Cat#MO20000
VIM	Cell Signaling Technology	Cat#5741
Thiophosphate ester	Dr. Kevan Shokat	110C
Normal rabbit IgG	Cell Signaling Technology	Cat#2729
Bacterial and Virus Strains		
Ad5-CMV-Cre	University of Iowa	VVC-U of Iowa-5
Escherichia coli (BL21)	New England Biolabs	Cat#C2530H
Biological Samples		

REAGENT or RESOURCE	SOURCE	IDENTIFIER
SCLC PDX: NJH29	(Jahchan et al., 2013)	N/A
SCLC PDX: JHU-LX102	(Leong et al., 2014)	N/A
SCLC PDX: JHU-LX92	(Poirier et al., 2015)	N/A
NSCLC PDX: JHU-LX55a	(Manchado et al., 2016)	N/A
NSCLC PDX: PDX727	Leanne Sayles and Alejandro Sweet-Cordero	N/A
NSCLC PDX: PDX0131	Leanne Sayles and Alejandro Sweet-Cordero	N/A
Chemicals, Peptides, and Recombinant Proteins		
JNS-140	(Grossman et al., 2017) and this paper	N/A
SMAP-1154	(Sangodkar et al., 2017)	N/A
SMAP-DT-061	(Sangodkar et al., 2017)	N/A
Cisplatin	Hospital Pharmacy	N/A
8-Br-cAMP	Tocris	Cat#1140
H89	Tocris	Cat#2910
Cantharidin	Tocris	Cat#1548
Critical Commercial Assays		
alamarBlue Cell Viability Reagent	Thermo Fisher	Cat#DAL1025
TruSeq Stranded Total RNA LT Kit	Illumina	Cat#15032612
ProtoScript cDNA Synthesis Kit	New England Biolabs	Cat#E6560L
Simple Western Quantitative Immunoassay (Wes) 12-230kDa Plates	ProteinSimple	Cat#SM-W004
Wes anti-rabbit secondary kit	ProteinSimple	Cat#DM-001
Wes anti-mouse secondary kit	ProteinSimple	Cat#DM-002
ApopTag Fluorescein In Situ Apoptosis Detection Kit	Millipore	Cat#S7110
Protein A-Agarose Fast Flow	Sigma-Aldrich	Cat#P3476
PKA Colorimetric Activity Kit	Thermo Fisher	Cat#EIAPKA
PP2A Immunoprecipitation Phosphatase Assay Kit	Millipore	Cat#17-313
SepPak C18 Column	Waters	Cat#WAT051910
nanoACQUITY UPLC System	Waters	Cat#17616
Thermo Q Exactive	Thermo Fisher	Cat# IQLAAEGAAPFALGMAZR
Deposited Data		
RNA sequencing data from SCLC xenografts expressing GFP or aPKA	This paper	GEO: GSE126353
Proteomics data: Kinome profiling of mouse and human SCLC tumors	This paper	ProteomeXChange PXD018209
Proteomics data: LAP-TAG purification of PKA interacting proteins	This paper	ProteomeXChange PXD017704
Proteomics data: AS-PKA covalent capture of PKA substrates	This paper	ProteomeXChange PXD018209
Proteomics data: Phosphoproteomic analysis of SCLC cells stimulated with 8-Br-cAMP	This paper	ProteomeXChange PXD018209
Experimental Models: Cell Lines		

REAGENT or RESOURCE	SOURCE	IDENTIFIER
Mouse: KP1	(Park et al., 2011)	N/A
Mouse: KP11	(Park et al., 2011)	N/A
Mouse: *Kras^{G12D};Trp53$^{-/-}$* lung adenocarcinoma cell lines	Leanne Sayles and Alejandro Sweet-Cordero	N/A
Human: A549	ATCC	CCL-185
Human: NCI-H69	ATCC	HTB-119
Human: NCI-H82	ATCC	HTB-175
Human: NCI-H187	ATCC	CRL-5804
Human: NCI-H446	ATCC	HTB-171
Experimental Models: Organisms/Strains		
Mouse: TKO model	(Schaffer et al., 2010)	N/A
Mouse: TKO;*Prkaca^{M120A}*	This paper	N/A
Mouse: TKO;*Gnas$^{flox/flox}$*	This paper	N/A
Mouse: *Gnas$^{flox/flox}$*	(Chen et al., 2005)	N/A
Mouse: B6.Cg-Gt(ROSA)26Sor$^{tm1(rtTA,EGFP)Nagy}$/J	The Jackson Laboratory	Stock No: 005670
Mouse: TKO;TetO7-*GNAS^{R201C}*	This paper	N/A
Mouse: TetO7-*GNAS^{R201C}*	(Iglesias-Bartolome et al., 2015)	N/A
Mouse:NOD.Cg-Prkdc^{scid}IL2rg^{tm1Wjl}/SzJ	The Jackson Laboratory	Stock No: 005557
Oligonucleotides		
Oligonucleotides for RT-qPCR, See Table S7	(Chen et al., 2005; Spandidos et al., 2010)	N/A
Oligonucleotides for shRNA, See Table S7	MISSION shRNA library; Sigma-Aldrich	N/A
Recombinant DNA		
Pet15B Prkaca expression vector	Dr. Susan Taylor	N/A
Pet15B Prkaca^{M120A} expression vector	This paper	N/A
Doxycycline-inducible active PRKACA expression vector (pLIX_402 backbone)	Dr. Robert Weinberg	N/A
Dox-inducible GFP control pLIX_403	(Lim et al., 2017)	N/A
pWPXLd/LAP-N/puro/DEST	This paper	N/A
pWPXLd	Dr. Didier Trono	Addgene #12258
pDONR223-PRKACA-WT	Jesse Boehm, William Hahn, David Root	Addgene #82311
pDONR221-PRKACB	Harvard PlasmID	HsCD00296755
pENTR221-PRKAR1A	Harvard PlasmID	HsCD00043858
Software and Algorithms		
ImageJ	ImageJ	https://imagej.nih.gov/ij/
ELDA	(Hu and Smyth, 2009)	http://bioinf.wehi.edu.au/software/elda/
DEseq2	(Love et al., 2014)	https://bioconductor.org/packages/release/bioc/html/DESeq2.html
Enrichr	(Chen et al., 2013)	https://amp.pharm.mssm.edu/Enrichr/

REAGENT or RESOURCE	SOURCE	IDENTIFIER
STAR2.5.1b	(Dobin et al., 2013)	https://github.com/alexdobin/STAR
Compass for Simple Western	Simple Western	https://www.proteinsimple.com/software_compass_simplewestern.html
Skyline	Schilling et al., 2012	https://skyline.ms/project/home/software/Skyline/begin.view
MSstats	(Choi et al., 2014)	https://www.bioconductor.org/packages/release/bioc/html/MSstats.html
Protein Prospector version 5.10.10	(Chalkley et al., 2008)	http://prospector.ucsf.edu/prospector/mshome.htm
WebLogo	(Crooks et al., 2004)	https://weblogo.berkeley.edu/logo.cgi
ClueGO version 2.5.3	(Bindea et al., 2009)	http://apps.cytoscape.org/apps/cluego
Cytoscape version 3.7	(Shannon et al., 2003)	https://cytoscape.org/
Metascape	(Zhou et al., 2019)	https://metascape.org/gp/index.html
Prism version 8.0.2	GraphPad	https://www.graphpad.com/scientific-software/prism/